Circadian desynchronization attenuates information throughput independent of daily rhythms in prefrontal cortex pyramidal neurons

Brandon L. Roberts[1], Jiexin Wang[1] and Ilia N. Karatsoreos[1]*

[1] Neuroscience and Behavior Program, and Department of Psychological and Brain Sciences, University of Massachusetts Amherst, Amherst, MA 01003, USA

Running Head: Daily rhythms in PFC

***Correspondence should be sent to:**

Ilia N. Karatsoreos, Ph.D.

Department of Psychological and Brain Sciences

University of Massachusetts Amherst

Tobin Hall, 135 Hicks Way

Amherst, MA 01003

E-mail: ikaratsoreos@umass.edu

Word count: Abstract (211), Introduction (470), Results (1,436), Discussion (2,229), Methods (1,060)

Figures: (9)

Figure supplements: (2)

Figure data files: (8)

Abstract

Circadian (daily) rhythms are ubiquitous in biology, from the molecular to behavioral levels. There is growing interest in understanding the functional implications and mechanisms of circadian oscillations in various neural systems, and the consequences of disrupted circadian rhythms on brain function due to our 24/7 modern environment. The prefrontal cortex (PFC) is heavily involved in myriad processes, including working memory, cognition, stress responses, and fear associated behaviors. Many PFC-associated behaviors are time-of-day dependent, yet how time-of-day impacts the fundamental function of neurons in the PFC and potential mechanism(s) by which this occurs remains unknown. Using patch-clamp electrophysiology, we demonstrate that the activity of prelimbic PFC neurons, their synaptic inputs, and action potential dynamics are regulated by time-of-day in a sex specific manner. Further, we show that in males, postsynaptic K^+ channels play a central role in mediating these rhythms, suggesting the potential for an intrinsic gating mechanism mediating information throughput. Finally, we demonstrate that environmental circadian desynchronization alters the intrinsic functioning of these neurons and decreases information throughput in part by altering GIRK1/2 channel function. These key discoveries in PFC physiology demonstrate the importance of understanding how daily rhythms contribute to the mechanisms underlying the basic functions of PFC circuitry, and how circadian disruption may impact fundamental properties of neurons.

Introduction

Circadian (daily) rhythms, imparted by an internal biological clock are ubiquitous in nature and play a central role in health and disease. Disruption of these clocks leads to myriad negative mental and physical health outcomes. Thus, it is crucial to understand the functional significance of circadian rhythms in neural function, particularly in higher brain areas.

The prefrontal cortex (PFC) serves as a critical component in cognition, emotional systems involved in fear learning and extinction, stress responses, and learning and memory, all of which vary over the course of the day [1–5]. The PFC is comprised of a wide array of cell types, including excitatory pyramidal neurons, which impact behavior by relaying information to other brain regions that are under clear circadian control, such as the amygdala and hippocampus, as well as inhibitory interneurons [6–9]. The prelimbic area (pl) of the PFC is divided into six distinct layers, each with distinct inputs and projections. Specifically, layer 2/3 plays a major role in working memory and behavioral plasticity and is involved in stress and depressive behaviors [7,10–12]. Notably, our previous work shows circadian desynchronization has profound impacts on the morphology of these plPFC pyramidal neurons [13].

plPFC pyramidal neurons receive excitatory glutamatergic and inhibitory GABAergic presynaptic inputs, with findings suggesting these are differentially regulated in male and female mice [3,9,14–16]. Excitatory inputs onto these neurons are plastic, with environmental factors such as stress, learning and memory leading to long-lasting potentiation of glutamatergic inputs onto these neurons through increased NMDAR- and AMPAR-mediated currents [10,17]. Over-activation of plPFC neurons is detrimental to normal behavioral function, and inhibitory inputs, which arise from the numerous inhibitory interneurons throughout the PFC, serve to modulate the excitability of PFC neurons [18]. The majority of PFC pyramidal neurons are intrinsically quiescent at rest and regulate information throughput via a wide array of ion channels, including cyclic-nucleotide-gated non-selective cation (HCN) channels, calcium (Ca^{2+}) and potassium (K^+) channels, including g-protein inward rectifying K^+ (GIRK) channels that mediate postsynaptic throughput of synaptic currents [11,19–21]. In the suprachiasmatic nucleus (SCN) brain clock, changes in sodium (Na^+), K^+, and Ca^{2+} ion channel function mediate daily rhythms in the spontaneous activity, and action potential dynamics of neurons [22,23]. How

67 these channels might impact daily rhythms in PFC function and the gating of information throughput is
68 unknown.

69 In the present study, we show that time-of-day clearly impacts the fundamental
70 neurophysiological properties of plPFC neurons. Second, we demonstrate that inhibitory and excitatory
71 synaptic inputs fluctuate throughout the day in a sex-dependent manner. Third, we identify that a
72 potential mechanism for these daily changes in information throughput in the plPFC involves K^+
73 channels. Lastly, we demonstrate that independent of time-of-day, circadian disruption decreases
74 information throughput in these neurons, in part, through altering GIRK channel function. Together, our
75 findings reveal that time-of-day is a critical factor that significantly changes information throughput in
76 plPFC pyramidal cells, and that these cells could be an important substrate for some of the negative
77 outcomes that accompany circadian desynchronization.

Results

Resting membrane potential of prelimbic layer 2/3 pyramidal neurons is rhythmic in male mice.

The regional and cell-specific heterogeneity in electrophysiological properties of PFC pyramidal neurons has been described in multiple species [11,24,25]. We observed two distinct phenotypes of plPFC pyramidal neurons that we categorized as type 1 and type 2, focusing these studies on the type 1 subset, which composed ~80% of recorded neurons (**Fig.1 Extended Data 1A-D**. The type 1 subset of layer 2/3 pyramidal neurons of the plPFC were identified visually by anatomical location and phenotypically by electrophysiological characterization in *ex vivo* coronal brain slices (**Fig. 1A, B;** *left*, **Fig.1 Extended Data 1A-D, Fig. 1 Extended Data 2A-I**). Pyramidal neurons were identified by shape and lucifer yellow (LY; 0.2%) was added to the patch pipette for confirmation of an apical dendrite (**Fig. 1B;** *right*).

To test our hypothesis that time-of-day impacts the basal electrophysiological properties of pyramidal neurons, we used whole-cell patch clamp techniques and measured resting membrane potential (RMP), membrane capacitance (Cm), and membrane resistance (Rm) at ZT bins: 0-4, 6-10, 12-16, and 18-22 in male (n = 6 mice/group) and female mice (n = 4-6 mice/group) (**Fig. 1A-G**). There was a main effect of time on RMP (no effect of sex) and interestingly, within group post-hoc analysis revealed that plPFC pyramidal neurons are more depolarized at ZT6-10 (light period) in male mice, when compared to 12-16 and 18-22 (dark period). Post-hoc analysis did not reveal a time-of-day effect on RMP in female mice (**Fig. 1D**). We did not observe an interaction between sex and time in any of our measures; however, there was a main effect of sex on Rm (**Fig. 1G**). Together, these data demonstrate that the RMP of plPFC pyramidal neurons in male mice changes throughout the light/dark (LD) cycle.

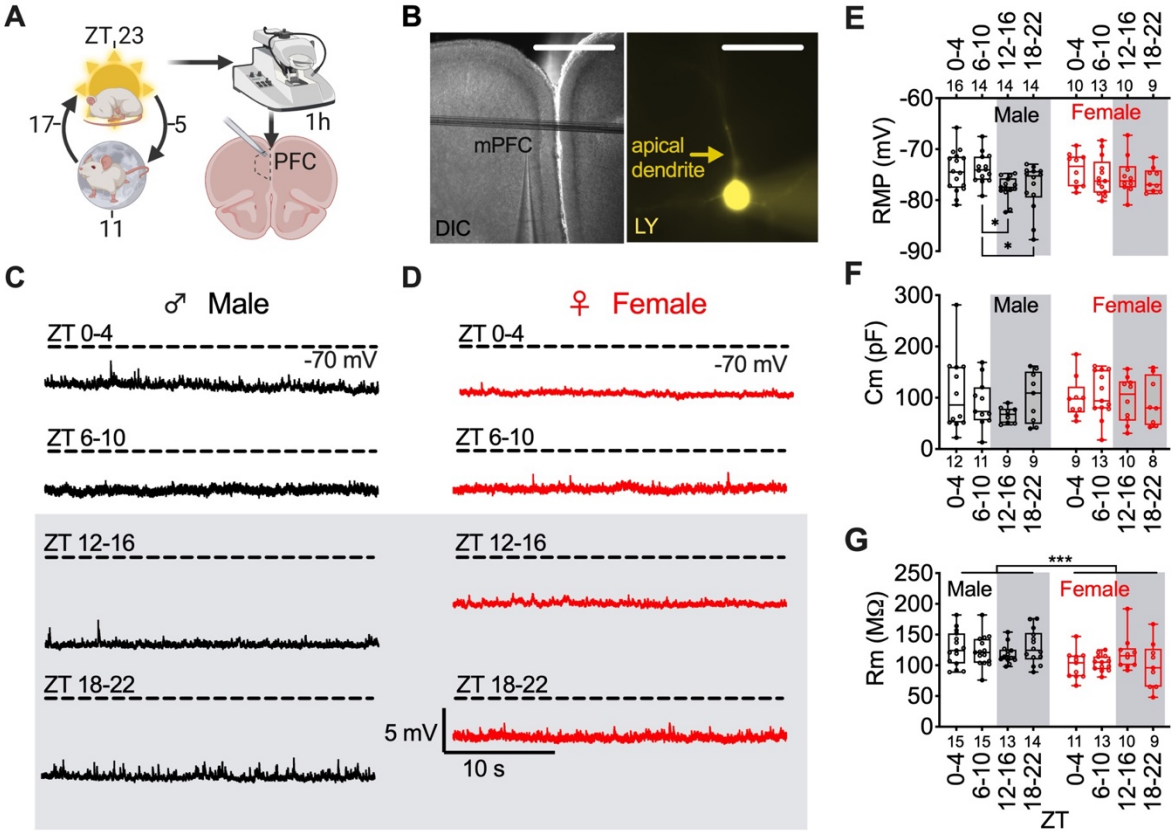

Figure 1. *Resting membrane potential of layer 2/3 mPFC pyramidal neurons is rhythmic in male mice.* **(A)** Diagram of methodological approach for ZT times (*left*) of *ex vivo* slice collection (*right*) **(B)** mPFC slice (*left;* scale 1mm) and layer 2/3 pyramidal neuron backfilled with lucifer yellow (LY, *right;* scale 10 µm). **(C)** Representative traces of current clamp recordings from male and **(D)** female mice at each ZT bin. **(E)** Mean and individual data points for membrane potential (RMP) at ZT0-4, 6-10, 12-16, and 18-22 in male (*black; left*) and female (*red; right*) mice (Time: F (3, 92) = 3.126; p = 0.03, sex: F (1, 92) = 0.718; p = 0.40) **(F)** Mean membrane capacitance (Cm; Time: F (3, 73) = 0.765, p = 0.52, sex: F (1, 73) = 0.430) and **(G)** resistance (Rm; Time: F (3, 92) = 0.250; p = 0.86, Sex: F (1, 92) = 13.25; p = <0.001) binned by ZT. Box plots represent median, min/max, and second and third quartiles**.** N-values for number of cells inset on x-axis. Two-way ANOVA for main effects and interaction with a within group Tukey post-hoc analysis for ZT bin, * $p < 0.05$, ***$p < 0.001$. Exact p-values, mouse N-values, and analysis in **Figure 1 – source data 1**.

103 **sEPSC activity on plPFC pyramidal neurons is increased during the active period in male mice**

104 Glutamatergic pyramidal neurons are the predominant cell-type in the plPFC, project to extra-
105 PFC cortical, subcortical and limbic regions, and interconnect within the PFC [26]. We hypothesized that
106 basal excitatory glutamatergic release contributes to daily changes in RMP and predicted that the
107 number and/or strength of excitatory inputs are highest during the light period, when plPFC pyramidal
108 neurons are depolarized (**Fig. 1C-E**). To test whether time-of-day alters excitatory inputs we used the
109 whole-cell voltage-clamp configuration (V_H = -70mV) to record sEPSCs in plPFC pyramidal neurons
110 from male (*n* = 6 mice/group) and female mice (*n* = 4-6 mice/group) at ZT0-4, 6-10, 12-16, and 18-22
111 (**Fig. 2A-G**). There was a main effect of ZT time on sEPSC frequency, but not amplitude, and post-hoc
112 analysis demonstrated that in male mice the frequency of excitatory inputs was increased early in the
113 dark period (ZT12-16), when RMP is hyperpolarized, an effect counter to our hypothesis (**Fig. 1B, 2A-**
114 **C**). Further, we observed clear sex differences on both sEPSC frequency and amplitude (*n* = 20-24
115 mice/group) (**Fig. 2D-G**). These data suggest that time-of-day impacts the number of excitatory inputs
116 (frequency), but not their strength (amplitude) in male mice.
117

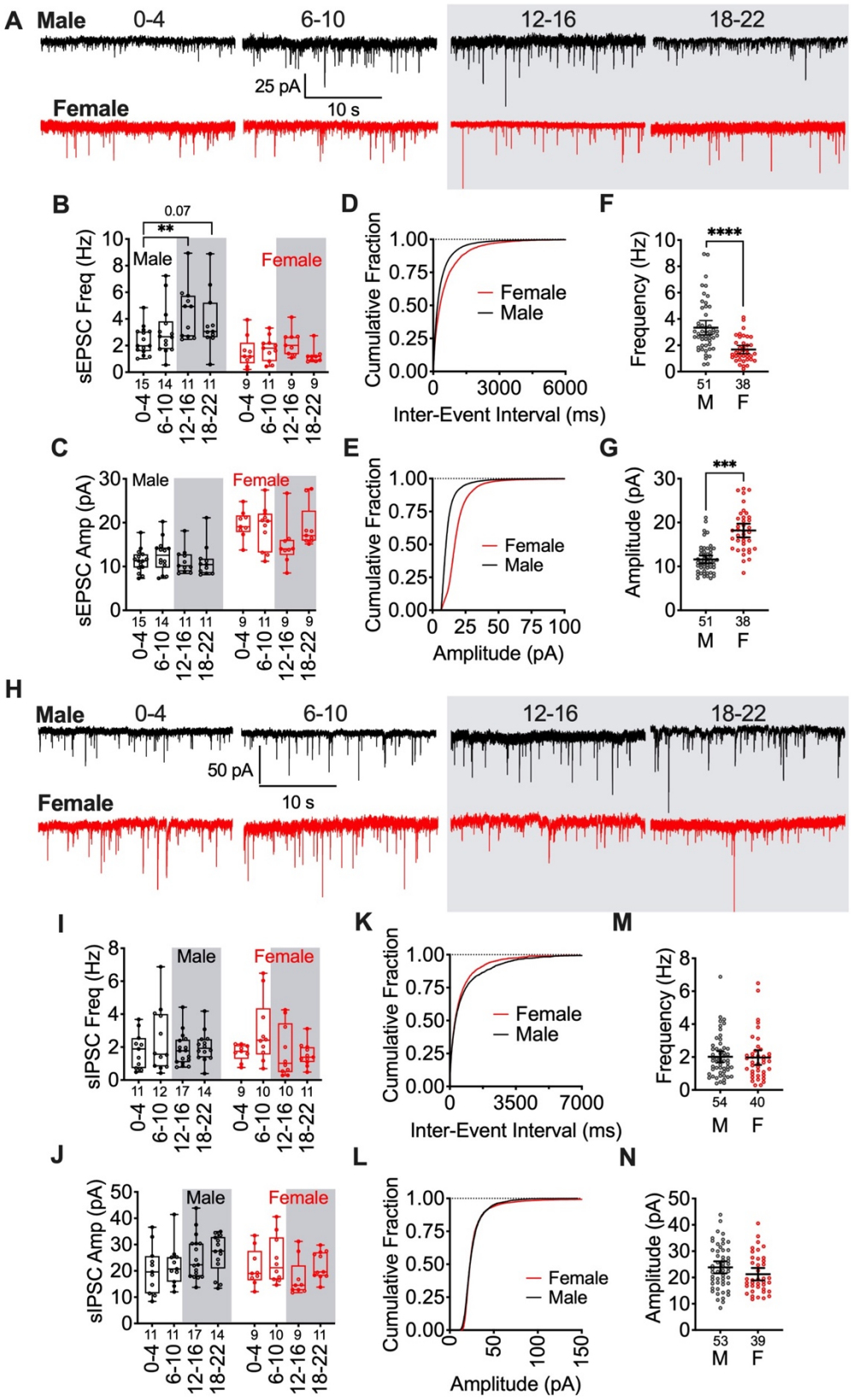
A
Male
0-4
6-10
12-16
18-22
25 pA
10 s
Female
B
0.07
**
sEPSC Freq (Hz)
Male
Female
15 14 11 11 9 11 9 9
0-4 6-10 12-16 18-22 0-4 6-10 12-16 18-22
C
sEPSC Amp (pA)
Male
Female
15 14 11 11 9 11 9 9
0-4 6-10 12-16 18-22 0-4 6-10 12-16 18-22
D
Cumulative Fraction
Female
Male
Inter-Event Interval (ms)
E
Cumulative Fraction
Female
Male
Amplitude (pA)
F
Frequency (Hz)
****
51 38
M F
G
Amplitude (pA)
***
51 38
M F
H
Male
0-4
6-10
12-16
18-22
50 pA
10 s
Female
I
sIPSC Freq (Hz)
Male
Female
11 12 17 14 9 10 10 11
0-4 6-10 12-16 18-22 0-4 6-10 12-16 18-22
J
sIPSC Amp (pA)
Male
Female
11 11 17 14 9 10 9 11
0-4 6-10 12-16 18-22 0-4 6-10 12-16 18-22
K
Cumulative Fraction
Female
Male
Inter-Event Interval (ms)
L
Cumulative Fraction
Female
Male
Amplitude (pA)
M
Frequency (Hz)
54 40
M F
N
Amplitude (pA)
53 39
M F

118

119

120

Figure 2. *Excitatory synaptic inputs onto plPFC pyramidal neurons are time-of-day dependent and differ by sex.* **(A)** Representative traces of sEPSC voltage clamp recordings from male (*top*) and female (*bottom*) mice at each ZT bin. **(B)** Mean sEPSC frequency (Time: F (3, 81) = 3.192; p = 0.028, Sex: F (1, 81) = 30.27; p = <0.0001) and **(C)** amplitude (Time: F (3, 81) = 2.019; p = 0.12, Sex: F (1, 81) = 62.79; p = <0.001) at ZT0-4, 6-10, 12-16, and 18-22. **(D)** Combined ZT cumulative fraction of inter-event interval and **(E)** amplitude in male and female mice. **(F)** Main effect of sex on mean sEPSC frequency and **(G)** amplitude. **(H)** Representative traces of sIPSC voltage clamp recordings from male (*top*) and female (*bottom*) mice at each ZT bin. **(I)** Mean sIPSC frequency (Time: F (3, 86) = 2.791; p = 0.045) and **(J)** amplitude (Time: F (3, 84) = 1.034; p = 0.38) at ZT0-4, 6-10, 12-16, and 18-22. **(K)** Combined ZT cumulative fraction of inter-event interval and **(L)** amplitude in male and female mice. **(M)** No main effect of sex on mean sIPSC frequency (Sex: F (1, 86) = 0.045, p = 0.83) and **(N)** amplitude (Sex: F (1, 84) = 2.094; p = 0.15). Box plots represent median, min/max, and second and third quartiles. N-values for number of cells inset on x-axis. Two-way ANOVA for main effects (including ***F, G, M*** *and* ***N***) and interaction, with a within group Tukey post-hoc analysis for ZT bin, *p < 0.05, **p < 0.01, ***p < 0.001. Exact p-values, mouse N-values, and analysis in **Figure 2 – source data 1**.

121

122 **Time-of-day does not alter sIPSCs in male or female mice**

123 Changes in RMP can be a consequence of intrinsic and/or synaptic properties. Our results on
124 sEPSC frequency and amplitude (**Fig. 2A-C**) in the plPFC suggest that excitatory synaptic inputs are
125 not the primary driver of the daily changes in RMP illustrated in **Fig. 1** and required further investigation
126 to identify the mechanism underlying time-of-day changes in resting state. We predicted that if synaptic
127 signaling is a primary mediator of time-of-day changes in RMP then inhibitory inputs should be robust
128 and highest during the dark period ZT bins. GABAergic interneurons make up a small portion of PFC
129 neurons, but are highly involved in the regulation of pyramidal neurons and relay information between
130 different regions within the PFC [9]. To determine if inhibitory inputs contribute to the diurnal tone of

131 pyramidal neurons, we recorded spontaneous inhibitory postsynaptic currents (sIPSCs; V_{Hold} = -70mV)
132 using a cesium (Cs^+) based internal solution in male (*n* = 6 mice/group) and female (*n* = 4 mice/group)
133 at ZT 0-4, 6-10, 12-16, and 18-22 (**Fig. 2H**). While there was a main effect of time on sIPSC frequency,
134 posthoc analysis did not reveal a significant difference in sIPSC frequency within groups (**Fig. 2I**) and
135 there was no main effect of ZT on sIPSC amplitude (**Fig. 2H-J**), but noted a trend in increased
136 amplitude prior to the dark period in male mice (**Fig. 2H-J**). There was no main effect of sex (*n* = 16-26
137 mice/group) on either reported measure (**Fig. 2M, N**). Overall, these data do not support the notion that
138 spontaneous synaptic inputs are the primary regulator of daily rhythms in neuronal resting state in
139 plPFC pyramidal neurons, and instead suggest a postsynaptic mechanism may regulate daily rhythms
140 in these neurons.
141
142 **mIPSCs onto plPFC pyramidal neurons are increased prior to the active period in female mice**
143 Our central goal was to identify the mechanism(s) by which daily rhythms impact information
144 throughput of plPFC pyramidal neurons. Given that we did not observe daily changes of RMP in female
145 mice, and there was a main effect of sex on membrane resistance (**Fig. 1E, G**), sEPSC frequency, and
146 amplitude (**Fig. 2F, G**) – all without an interaction between sex and ZT bin – we proceeded with our
147 mechanistic investigation by separating male and females into independent groups.
148 Although we did not observe a main effect of ZT bin on sIPSC amplitude, there was a main
149 effect of time on sIPSC frequency **(Fig. 2I).** Further, when ZT bins were combined into light period and
150 dark period, we identified a near significant impact of the LD cycle on sIPSC amplitude in male mice
151 (*data not shown;* t = 1.981*, df = 51; p* = 0.053). To further investigate whether time-of-day impacts the
152 presynaptic or postsynaptic components of inhibitory inputs, we measured mIPSCs by bath applying
153 the voltage-gated sodium channel blocker tetrodotoxin (TTX), which isolates the synapse from
154 upstream activity by inhibiting action potential firing. We observed no effect on mIPSC frequency, which
155 is typically associated with presynaptic neurotransmitter release, in male mice (*n* = 6-8 mice/group)
156 (**Fig. 3A, B**). Although we did not observe time-of-day changes in mIPSC amplitude, decay tau or total
157 area (**Fig. 3C-E**), there was a trend of decreased decay tau during the dark period (**Figure 3D**).

158 Notably, in female mice (*n* = 4 mice/group) we did observe an increase in mIPSC frequency and
159 amplitude during the latter part of the light period (ZT 6-10; **Fig. 3F-H**). Further, although there was no
160 effect on decay tau, the total mIPSC area was also increased at ZT6-10 (**Fig. 3I, J**). Combined, these
161 data show that inhibitory inputs onto plPFC pyramidal neurons are not rhythmic in male mice, but there
162 are trends in post-synaptic measures such as sIPSC amplitude and mIPSC decay tau. Further, multiple
163 post-synaptic components mediating throughput of inhibitory inputs (mIPSC amplitude and total area)
164 were dependent on time-of-day in female mice (**Fig. 3H, J**).
165

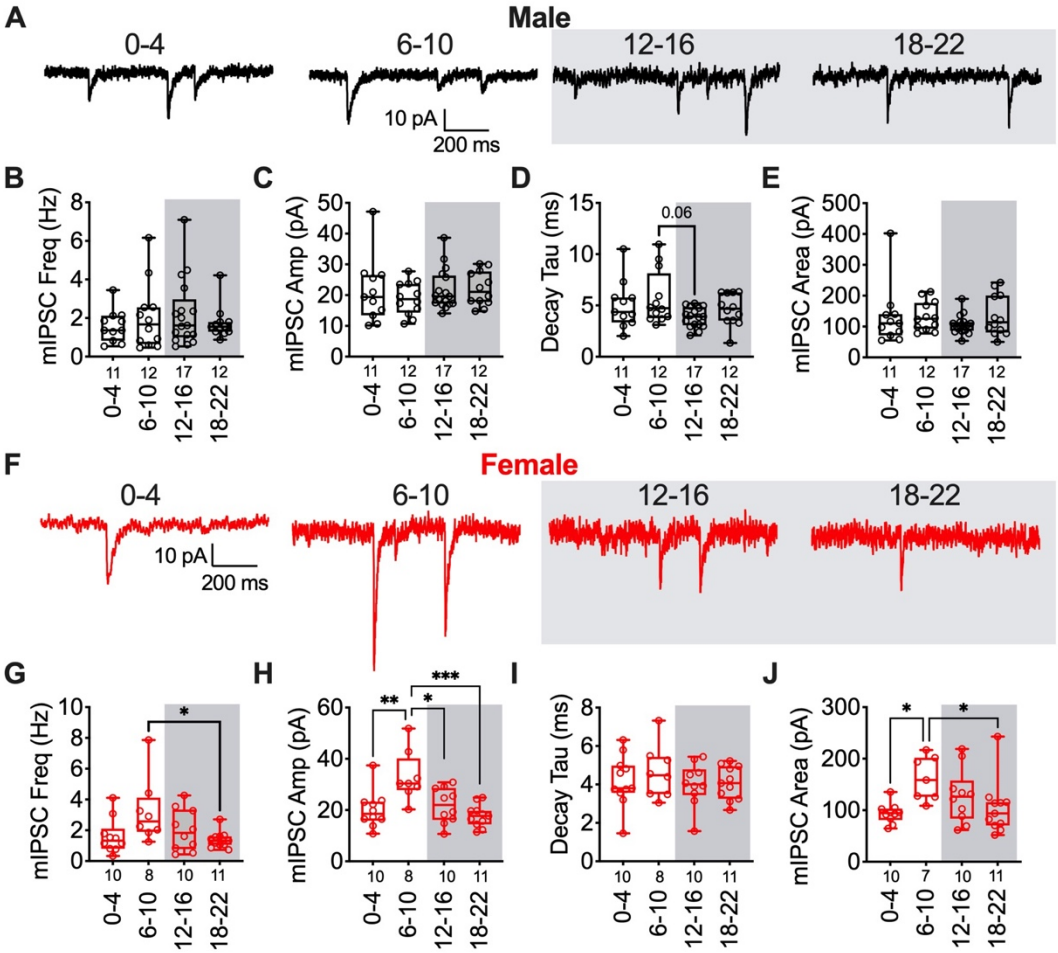

166

Figure 3. *Strength of inhibitory synaptic inputs onto plPFC pyramidal neurons are increased prior to the active period in female mice.* **(A)** Representative traces of mIPSC voltage clamp recordings from male and **(F)** female mice at each ZT bin. **(B, G)** Mean mIPSC frequency (Male: F (3, 48) = 0.562; p = 0.64, Female: F (3, 35) = 3.323; p = 0.03), **(C, H)** amplitude (Male: F (3, 48) = 0.5084, p = 0.678355, Female: F (3, 35) = 7.938; p = <0.001), **(D, I)** decay tau (Male: F (3, 48) = 2.444; p = 0.08, Female: F (3, 36) = 0.4939; p = 0.69), and **(E, J)** total area (Male: F (3, 48) = 0.7413; p = 0.5327, Female: F (3, 34) = 3.829; p = 0.02) at ZT0-4, 6-10, 12-16, and 18-22 in male (*black; top*) and female (*red; bottom*) mice. Box plots represent median, min/max, and second and third quartiles. N-values for number of cells inset on x-axis. One-way ANOVA with Tukey post-hoc analysis for ZT bin, *p < 0.05, **p < 0.01, ***p < 0.001. Exact p-values, mouse N-values, and analysis in **Figure 3 – source data 1**.

167 **Membrane conductance is increased prior to the inactive period in female mice**

168 Multiple components of mIPSCs were enhanced during the latter portion of the light period
169 (ZT6-10) in female mice (*n* = 4 mice/group), suggesting that post-synaptic cell endogenous properties
170 may mediate daily rhythms of the physiological properties in plPFC pyramidal neurons. To investigate
171 any potential daily changes in postsynaptic properties, we used a potassium (K^+) gluconate internal
172 solution and measured the current-voltage (I-V) relationship in these neurons by performing a voltage-
173 step inactivation protocol in which neurons held at -70mV were depolarized to 30mV and
174 hyperpolarized in 10mV steps to a final MP of -120mV (**Fig. 4A, B**). We analyzed the delayed steady-
175 state current density (current density = (I_{Total})/(Cm)) during the hyperpolarized (from -120 mV to -70mV
176 (*K1*); **Fig. 4A-C**) and depolarized state (0 mV to 30mV (*K2*); **Fig. 4A, B, E**), as well as daily changes in
177 normalized conductance (g) calculated as the slope of the K1 and K2 steady-state current normalized
178 to cell capacitance: $g_{Normalized} = ((I_{VH2} – I_{VH1}) / (V_H2 – V_H1))/(Cm)$, at different ZT bins (**Fig. 4D, F**). We
179 observed a main time-of-day effect (*n* = 4-6 mice/group) on current density and normalized
180 conductance for the K1 hyperpolarized voltage steps, although there was no main effect at the K2
181 depolarized voltage steps (**Fig. 4B-F**). Together, these data demonstrate that female mice do indeed
182 display daily rhythms in postsynaptic membrane properties, but they are not robust enough to alter
183 resting state (**Fig. 1D, E**).
184

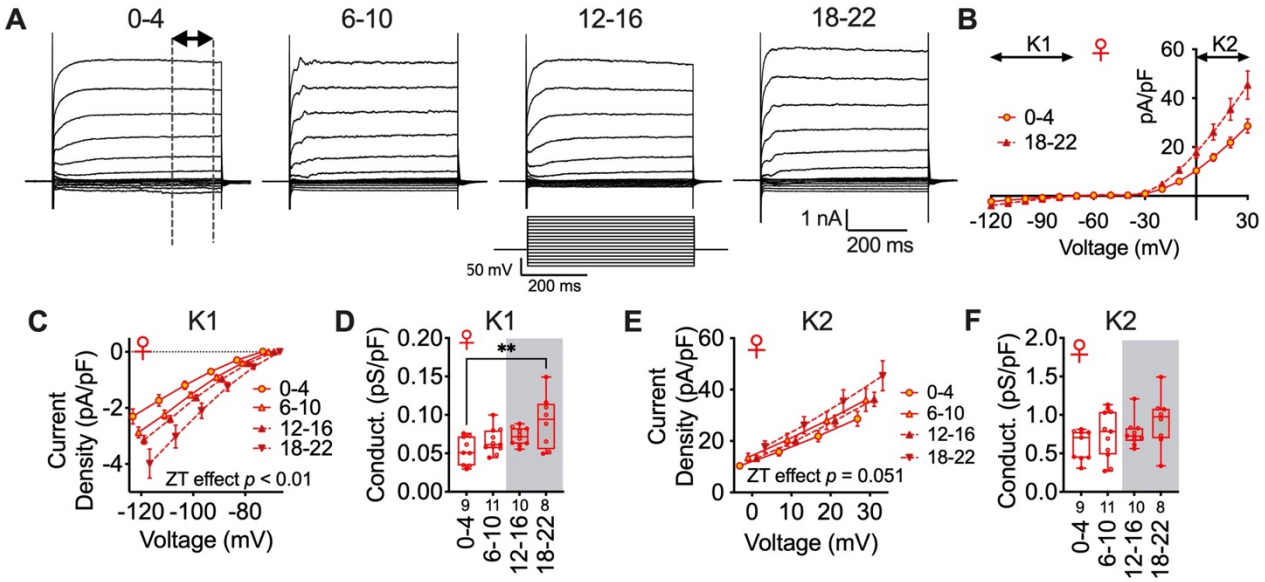

185

Figure 4. *Membrane conductance at hyperpolarized voltages is increased during the active period in female mice.* **(A)** Current-voltage trace (*top; dashed line represents steady state current averaged for analysis*) after voltage-step protocol (*bottom middle*). **(B)** Averaged I-V voltage-step relationship from -120 mV to 30 mV for ZT0-4 and 18-22 (*normalized to cell capacitance*) with a K^+ internal solution. **(C, E)** Current density (K1 (time): F (3, 34) = 5.425; p = 0.0037, K2 (time): F (3, 34) = 2.869; p = 0.0508) and **(D, F)** conductance of K1 (F (3, 34) = 4.900; p = 0.006) and K2 (F (3, 34) = 1.938; p = 0.14) currents (*respectively*) at ZT0-4, 6-10, 12-16, and 18-22 in female mice. K1 and K2 represent hyperpolarized and depolarized currents (*respectively*). Box plots represent median, min/max, and second and third quartiles. Error bars on I-V plots represent ± SEM. N-values for number of cells inset on bars. Two-way ***(C, E)*** or One-way ***(D, F)*** ANOVA with Tukey post-hoc analysis for ZT bin. ***p* < 0.01. Exact p-values, mouse N-values, and analysis in **Figure 4 – source data 1**.

186 **K+ channel activity regulates postsynaptic rhythmic activity in pyramidal neurons of male mice**

187 Given that synaptic inputs are rhythmic in male and female mice, but only male mice display
188 daily rhythms in RMP, we hypothesized that changes in postsynaptic ionic currents, as measured by
189 the I-V relationship, may play a role in setting the functional tone of plPFC pyramidal neurons in male
190 mice. As in **Fig. 4**, we analyzed the I-V relationship by running a voltage-step protocol (**Fig. 5A, B**). In
191 male mice (*n* = 6 mice/group) the I-V relationship demonstrated a clear inward rectifying current at
192 lower holding voltages and a delayed rectifying current at depolarizing voltages, resulting in a larger
193 current density early in the dark period (ZT12-16) in both the hyperpolarized (**Fig. 5A-C**) and
194 depolarized state (**Fig. 5A, B, D**). This effect translated into higher normalized cell conductance late in
195 the light period and early in the dark period (**Fig. 5I, J)**.

196 Since ionic conductance was highest at ZT12-16, the same ZT bin that RMP was most
197 hyperpolarized (**Fig.1E**), we predicted that this increase involved anionic ion channel activity that
198 results in a net negative current. Further, in the hyperpolarized state, the current density at each ZT
199 began to converge near our calculated reversal potential for K^+. To determine if daily changes in current
200 density and normalized cell conductance was dependent on K^+ channel activity, we utilized a K^+ free
201 Cs^+-based internal recording solution to block outward K^+ currents (*n* = 6-8 mice/group). This
202 preparation completely abolished the time-of-day effect on current density at lower holding voltages, but
203 not in the depolarized state (**Fig. 5E-H**). Further, the time-of-day effect on normalized cell conductance
204 was blocked when calculated at the presented voltages with a main effect of Cs^+ on overall
205 conductance in the depolarized state (**Fig. 5I,J**). Of particular note, blockade of outward K^+ currents via
206 internal Cs^+ appeared to have little effect at ZT0-4, suggesting minimal K^+ channel activity at this ZT bin
207 (**Fig. 5C,G**). Together, these data demonstrate that ion channel activity is time-of-day dependent in
208 plPFC pyramidal neurons and K^+ channels contribute to daily rhythms in their cellular conductance.
209

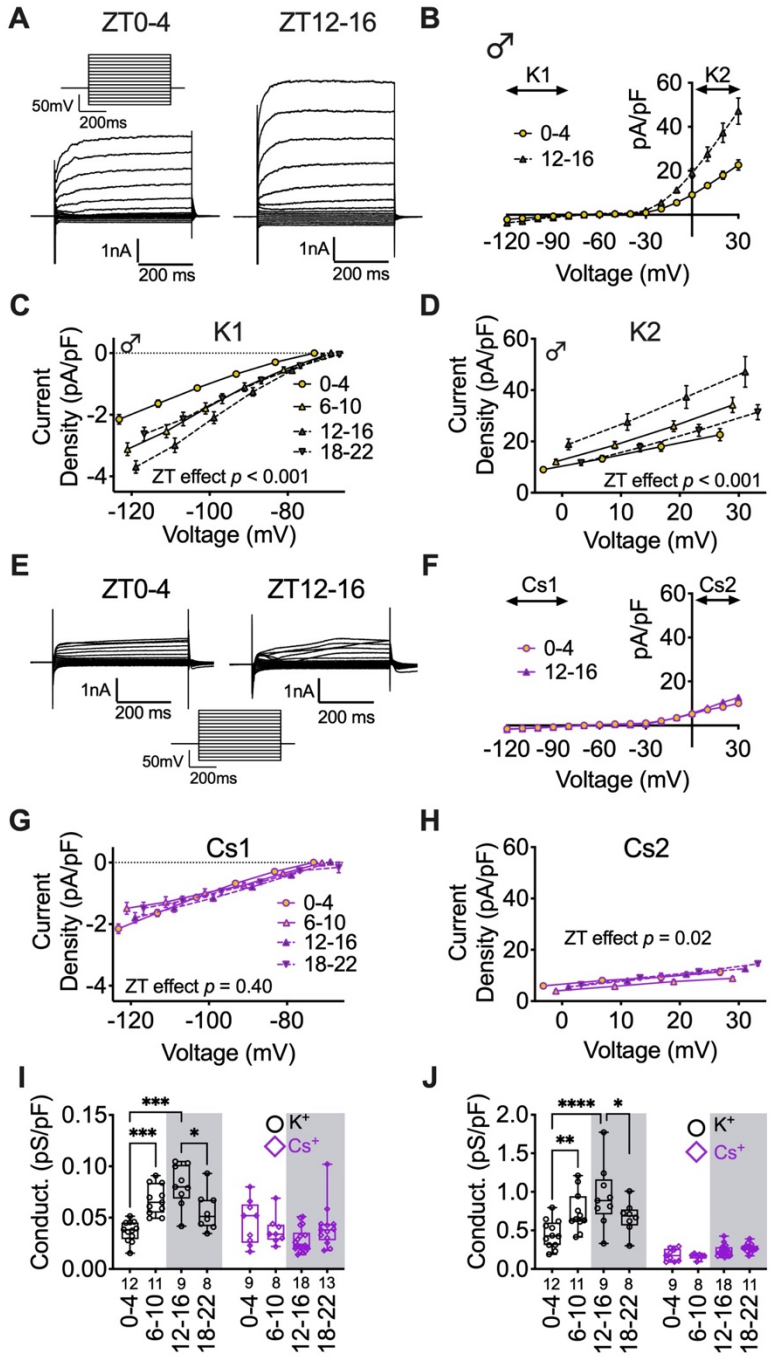
A
ZT0-4
ZT12-16
50mV
200ms
1nA
200 ms
B
♂
K1
K2
0-4
12-16
pA/pF
Voltage (mV)
C
K1
Current Density (pA/pF)
0-4
6-10
12-16
18-22
ZT effect p < 0.001
Voltage (mV)
D
K2
ZT effect p < 0.001
Voltage (mV)
E
ZT0-4
ZT12-16
F
Cs1
Cs2
G
Cs1
ZT effect p = 0.40
H
Cs2
ZT effect p = 0.02
I
Conduct. (pS/pF)
K+
Cs+
J

210

Figure 5. *K^+ channels are required for time-of-day effects on membrane conductance.*

(A) Voltage-step protocol (*top left*) and representative voltage-step traces of I-V relationship at ZT 0-4 (*left*) and 12-16 (*right*) in male mice. **(B)** Averaged I-V relationship for ZT0-4 and 12-16 (*normalized to cell capacitance*) with a K^+ internal solution. **(C)** Current density of K1 (Time: F (3, 37) = 9.115; p = <0.001) and **(D)** K2 (Time: F (3, 37) = 9.055; p = <0.001) I-V relationships at ZT0-4, 6-10, 12-16, and 18-22. **(E)** Representative voltage-step traces of **(F)** I-V relationship at ZT 0-4 (*left*) and 12-16 (*right*) with a Cs+ internal solution. **(G)** Current density of Cs1 (Time: F (3, 48) = 1.009; p = 0.40) and **(H)** Cs2 (Time: F (3, 45) = 3.540; p = 0.02) I-V relationships at each ZT bin. **(I)** Comparison each ZT bin for K1 and Cs1 (Time: F (3, 80) = 2.682; p = 0.05, Internal: F (1, 80) = 37.22; p = <0.001), and **(J)** K2 and Cs2 (Time: F (3, 81) = 7.896; p = 0.0001, Internal: F (1, 81) = 141.1; p = <0.0001) normalized cell conductance. Two-way ANOVA for main effects and interaction, with a within group Tukey post-hoc analysis for ZT bin, voltage, and internal solution. Box plots represent median, min/max, and second and third quartiles. Error bars on I-V plots represent ± SEM. N-values for number of cells inset on x-axis. *p < 0.05, **p < 0.01, ***p < 0.001, ****p < 0.0001. Exact p-values, mouse N-values, and analysis in **Figure 5 – source data 1**.

Information throughput is decreased during the active period in plPFC pyramidal neurons

To understand the functional implications of daily rhythms in RMP and postsynaptic ion channel function for information throughput, we tested how time-of-day impacts action potential dynamics. We utilized a 10-pA current injection protocol to evoke action potentials at ZT0-4, 6-10, 12-16, and 18-22 and observed a main effect of time for membrane potential threshold of action potential firing, with post-hoc analysis revealing an increased threshold for firing late in the dark period (ZT18-22) when compared to ZT6-10 in male mice (n = 6 mice/group) (**Fig. 6A-C**). Consistent with the null effect of time on RMP in female mice, there was no effect of time on action potential threshold (n = 4-6 mice/group) (**Fig. 6C**). Further, although there was no effect on amount of current needed to elicit an action potential (rheobase) in male mice, once rheobase was reached, subsequent current injections evoked action potential firing at a lower frequency during the dark period (**Fig. 6D, E**). Although we did not observe a

time-of-day effect on action potential amplitude or half-width in male mice (**Fig. 6F-G**), decay tau, a component of action potential firing that is modulated to a large extent by K^+ channels, was reduced at ZT18-22 (**Fig. 6E**). These data suggest that plPFC pyramidal neurons are not only more hyperpolarized during the light period, but are functionally more difficult to activate, requiring larger depolarizations to elicit action potentials and relay information downstream.

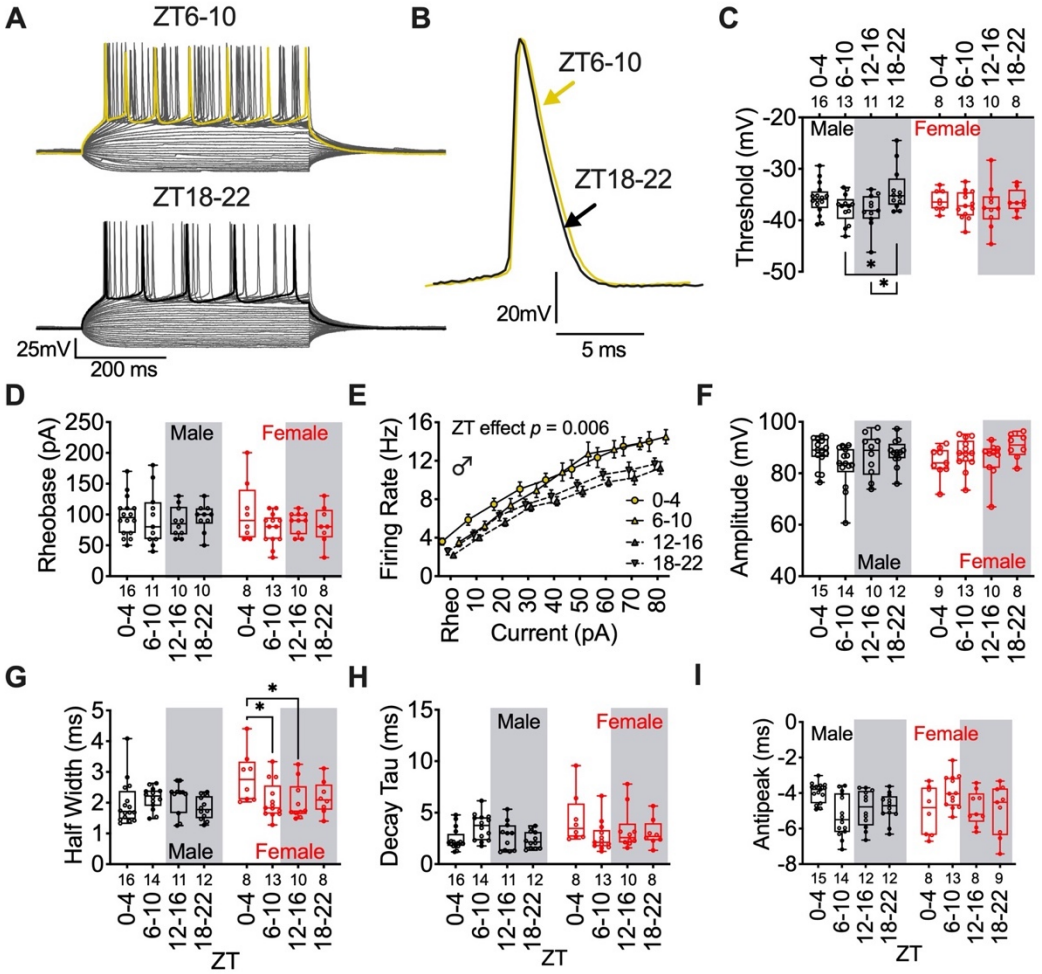

Figure 6. *Information throughput is decreased during the active period in male mice.* **(A)** Representative trace of current step recording with maximal AP firing highlighted at ZT6-10 (*top; yellow*) and 18-22 (*bottom; black*) and **(B)** individual evoked APs in male mice. **(C)** Mean AP threshold (Time: F (3, 83) = 2.809; p = 0.04, Sex: F (1, 83) = 0.1388; p = 0.71) **(D)** Rheobase (Time: F (3, 78) = 0.9519; p = 0.42, Sex: F (1, 78) = 0.6786; p = 0.41), **(E)** evoked firing rate (from rheobase; male mice Time: F (3, 41) = 4.815; p = 0.006), **(F)** amplitude (Time: F (3, 83) = 1.489; p = 0.22, Sex: F (1, 83) = 0.1132; p = 0.74), **(G)** half width (F (3, 84) = 1.993; p = 0.12, Sex: F (1, 84) = 4.045; p = 0.049), **(H)** decay tau (Time: F (3, 84) = 0.7564; p = 0.5217, Sex: F (1, 84) = 3.442; p = 0.0671) and **(I)** antipeak (Time: F (3, 84) = 0.8137; p = 0.49, Sex: F (1, 84) = 0.0505; p = 0.82) at each ZT bin in male and female mice. Box plots represent median, min/max, and second and third quartiles. Error bars on I-V plots represent ± SEM. N-values for number of cells inset on x-axis. Two-way ANOVA for main effects and interaction, with a within group Tukey post-hoc analysis for ZT bin and/or current injection. *p <0.05.* Exact p-values, mouse N-values, and analysis in **Figure 6 – source data 1**.

228

229 **Circadian disruption decreases information throughput in PFC pyramidal neurons**

230 Environmental circadian desynchronization (ECD) by housing in an altered 10:10h light:dark cycle,
231 negatively impacts cognitive flexibility and alters both morphology and dendritic connections of layer 2/3
232 plPFC pyramidal neurons in mice [13]. We hypothesized that the impact of ECD on these neurons would
233 extend to their endogenous physiological properties. Using the 10:10h light:dark cycle to induce ECD,
234 we measured changes in resting state properties and action potential dynamics at ZT6-10 and 18-22
235 (calculated as 50min/h in ECD mice; **Fig. 7A-J**), which were the ZT bins that displayed the largest
236 difference in action potential firing threshold under non-ECD conditions (**Fig. 6A-C**). We did not observe
237 main effects of time or ECD on membrane resistance or capacitance, although there was a trend
238 towards decreased membrane resistance in ECD mice (**Fig. 7C, D**). However, there was a main effect
239 of ECD, independent of time-of-day, on the resting membrane potential and action potential firing
240 threshold (**Fig. 7E, F**). Further, ECD had a main effect on all components of action potential dynamics

that were measured, including half width, decay tau, amplitude, and antipeak (**Fig. 7A-B, F-J**). Lastly, any effects of time observed in control mice, such as action potential threshold and decay tau, was lost in ECD mice. While there was no ECD effect on rheobase or action potential firing rate after current injection (**Fig. 7K-L**), these parameters were also not different at these ZT bins in non-ECD conditions (**Fig. 7D-E**) They also do not account for the significant increase in the number of neurons that did not elicit action potentials (quiescent) after our current injection protocol in ECD mice (**Fig.7M**). Together these data show that independent of time-of-day, ECD alters the fundamental intrinsic properties of pIPFC pyramidal neurons.

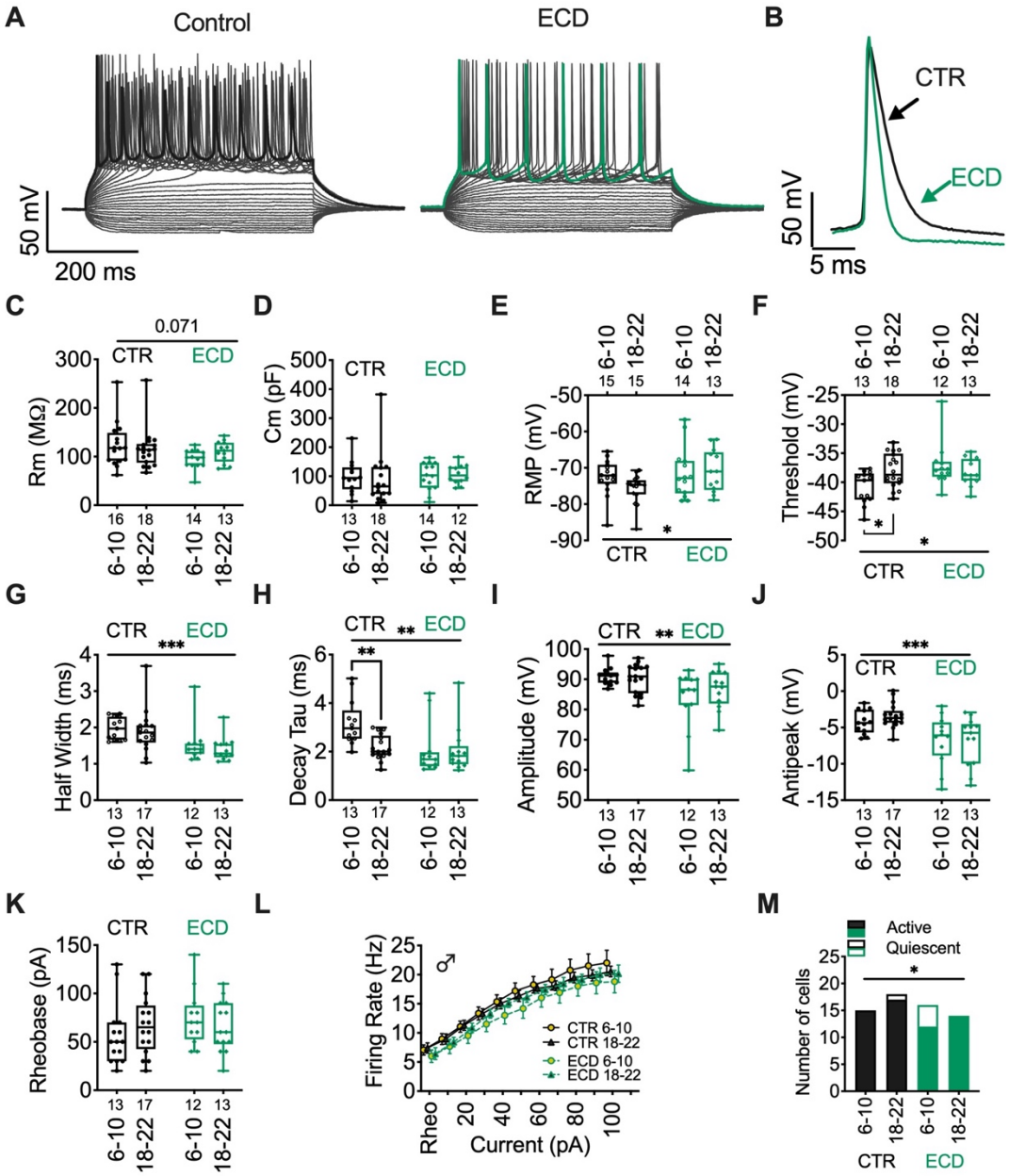

Figure 7. *Environmental Circadian Desynchronization decreases information throughput and alters fundamental properties of PFC pyramidal neurons independent of time-of-day.* **(A)** Representative trace of current step recording with maximal AP firing and **(B)** individual evoked APs highlighted at ZT6-10 in control (CTR) (*left; black*) and ECD (*right; bluish green*) in male mice. **(C)** Mean resting membrane resistance (Time: F (1, 57) = 0.1405, p = 0.7092, Treatment: F (1, 57) = 3.384; p = 0.071) **(D)** capacitance (Time: F (1, 51) = 0.0009; p = 0.98, Treatment: F (1, 51) = 0.2443; p = 0.62), **(E)** membrane potential (Time: F (1, 52) = 0.9617; p = 0.33, Treatment: F (1, 52) = 4.275, p = 0.04), **(F)** action potential firing threshold (Time: F (1, 52) = 1.1143; p = 0.29, Treatment: F (1, 52) = 4.867; p = 0.03), **(G)** half width (Time: F (1, 51) = 0.8106; p = 0.37, Treatment: F (1, 51) = 13.80; p < 0.001), **(H)** decay tau (Time: F (1, 51) = 4.705; p = 0.0348, Treatment: F (1, 51) = 7.294; p = 0.0094) , **(I)** amplitude (Time: F (1, 51) = 0.4232; p = 0.52, Treatment: F (1, 51) = 10.24; p = 0.002), and **(J)** action potential antipeak (Time: F (1, 51) = 0.292; p = 0.5913, Treatment: F (1, 51) = 17.70; p = 0.0001) at ZT 6-10 and 18-22 in male mice. **(K)** Mean rheobase (Time F (1, 53) = 0.0125; p = 0.91, Treatment: F (1, 53) = 1.081; p = 0.30) **(L)** Firing rate (F (3, 54) = 0.832; p = 0.48), Treatment: F (1, 53) = 1.081; p = 0.30) and **(M)** number of active vs quiescent neurons after 200pA current injection. Box plots represent median, min/max, and second and third quartiles. N-values for number of cells inset on x-axis. Two-way ANOVA for main effects and interaction, with Šídák's multiple comparisons post-hoc analysis for ZT bin. *$^{*}p < 0.05$, $^{**}p < 0.01$, $^{***}p < 0.001$.* Exact p-values, mouse N-values, and analysis in **Figure 7 – source data 1.**

Circadian disruption upregulates GIRK1 channel activation independent of daily rhythms

Our previous work showed that ECD impacts the PFC by reducing pyramidal cell dendritic arborizations and impairs cognitive flexibility[13]. Notably, G protein-gated inwardly rectifying K^+ (GIRK) channels throughout the PFC contribute to the regulation of cognitive flexibility [15,27,28]. To test if GIRK1 (Kir3.1) channel function contributes to decreased information throughput in ECD mice independent of time-of-day, we evoked action potentials before and after the bath application of the selective GIRK1 channel agonist ML297 (10 μM)[28,29] (**Fig. 8A, B**). Compared to control mice, most neurons recorded from ECD

257 mice failed to elicit action potentials in the presence of ML297 irrespective of the light/dark period (**Fig.**
258 **8C**). To specifically measure the chronic impact of ECD on pyramidal neuron function, we combined
259 both ZT groups to eliminate time-of-day as an independent variable. In control mice, activation of
260 GIRK1/2 channels did increase the threshold of action potential firing, suggesting that GIRK channels
261 are functional in control and ECD mice, but their impact on cellular function and inhibition of information
262 throughput is more robust in ECD mice (**Fig. 8C, D**). To test if GIRK channels differentially alter cellular
263 conductance in hyperpolarized states (-110 to -40 mV) that are associated with GIRK activation[30], we
264 used a voltage-step protocol to measure the current-voltage relationship before and after application of
265 the selective ML297 (10 μM) (**Fig. 8E, F**). Confirming that GIRK channels are functional in both CTR
266 and ECD, ML297 induced GIRK activation increased the slope of the I-V relationship, representative of
267 increased K^+ conductance (**Fig. 8E, F**). To determine if currents attributed to GIRK channel activation
268 were larger in ECD mice, we isolated ML297 induced currents ($I_{ML297+acSF} - I_{aCSF} = I_{ML297}$) and showed
269 that GIRK channel conductance is upregulated in ECD mice. Together, these data demonstrate that
270 GIRK channel activity contributes to changes in information throughput induced by ECD.

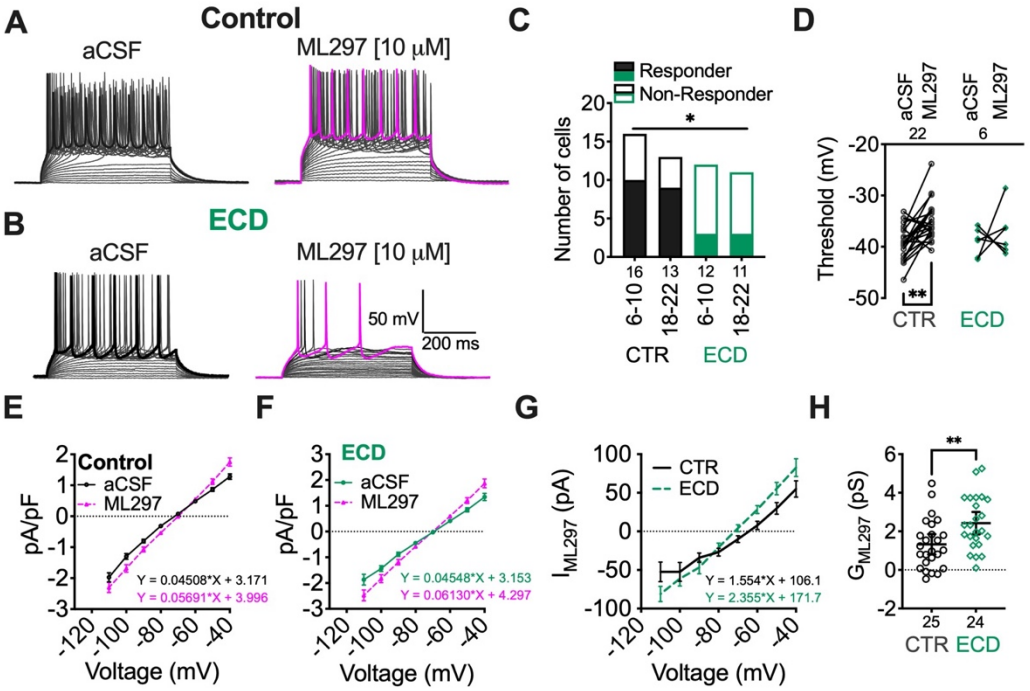

Figure 8. *Circadian disruption increases GIRK1/2 channel conductance in PFC pyramidal neurons.* **(A)** Representative trace of current step recording with maximal AP firing highlighted in control (CTR) and **(B)** ECD before (*left*) and after (*right*) application of ML297 (10 μM) in male mice. **(C)** Number of cells that elicited action potentials in the presence of ML297 (Chi-square = 8.131, df = 3; $p = 0.043$) and **(D)** threshold of action potential firing for responsive cells (Two-way ANOVA, Drug: F (1, 26) = 6.457; $p = 0.02$, Light Period: F (1, 26) = 0.7953; $p = 0.34$). **(E)** Current voltage plot in 10mV steps from -110 to -40 mV before and after application of ML297 in CTR (Regression, F(1, 364) = 42.79; $p < 0.001$) and **(F)** ECD mice (Regression, F(1, 388) = 41.20; $p < 0.001$). **(G)** Mean ML297 induced current in CTR and ECD mice (Regression, F(1, 348) = 19.27; $p < 0.001$) **(H)** Conductance of ML297 induced currents (Unpaired t-test; t = 2.881, df = 47, $p = 0.006$). Error bars represent ± SEM. N-values for number of cells inset on x-axis. *$p < 0.05$, **$p < 0.01$, ***$p < 0.001$. Exact p-values, R^2, mouse N-values, and analysis in **Figure 8 – source data 1.**

Discussion

The suprachiasmatic nucleus (SCN) is the central circadian clock in mammals and regulates daily changes in gene expression and activity throughout the brain [31]. However, it has become clear that numerous brain regions display daily rhythms. A major hypothesis in the field is that these extra-SCN clocks and the SCN operate synergistically to drive daily rhythms in nearly all components of physiology and behavior, which is why their disruption has numerous physiological and psychological consequences, including exacerbated metabolic and mood disorders [2,32–35]. While there have been several well executed studies that demonstrate the presence of daily rhythms in neurophysiological function in the hippocampus and brainstem, none have included the PFC, and all have largely focused on extracellular field recordings [36–40]. Thus, previous studies have not shed light on the fundamental electrophysiological processes at the cellular level that are affected by time-of-day in higher brain areas.

In this study we present five main findings (**Fig. 9**). First, layer 2/3 plPFC pyramidal neurons in male mice are hyperpolarized during the early portion of the dark period when compared to the latter portion of the light period. Second, time-of-day impacts excitatory and inhibitory inputs onto plPFC pyramidal neurons, with clear sex differences in excitatory inputs. Third, we demonstrate that male mice display distinct changes in ion channel activity and action potential kinetics, with male mice showing increased action potential firing threshold and decreased decay tau during portions of the dark period. Fourth, we identify that changes in K^+ channel activity serves as a potential mechanism underlying time-of-day changes in the RMP and action potential firing rates of plPFC pyramidal neurons. Finally, we illustrate that circadian desynchronization disrupts multiple properties of neural function, reduces information throughput, and alters GIRK channel function (**Fig. 9**). By identifying the intrinsic properties and synaptic inputs of plPFC pyramidal neurons, and a putative cellular substrate for the effects of circadian desynchronization, these findings allow us to better understand the relationship between circadian function/dysfunction, intrinsic PFC circuitry and its outputs.

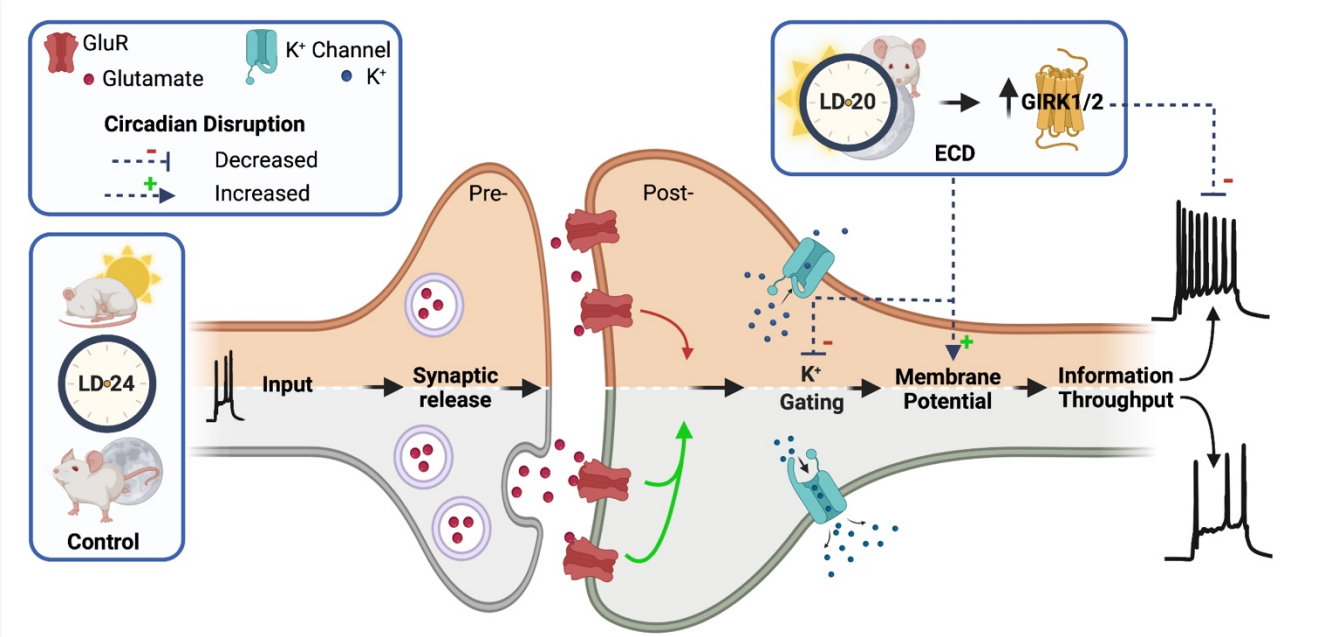

Figure 9. *Model highlighting daily rhythms of information throughput in mPFC pyramidal neurons and the impact of circadian disruption on these neurons.* Synapse representing functional throughput in the inactive (*top*) and active (*bottom)* period in male mice. Presynaptic activity (*left*) results in an increase of excitatory glutamatergic release onto layer 2/3 plPFC pyramidal neurons during the active period. Postsynaptic (*right*) changes in K^+ channel activity contribute to the basal conductance and excitability of these neurons. Further, changes in membrane potential and action potential firing threshold result in a net decrease of information throughput during active period. Independent of time of day (*upper right*), ECD has a depolarizing effect on these neurons, decreases components of action potential dynamics associated with voltage-gated K+ channel function, and induces an increase in GIRK1/2 channel conductance, resulting in an overall decrease in information throughput.

298

299 Changes in PFC function underly numerous psychiatric disorders including bipolar, post-
300 traumatic stress disorder (PTSD), attention deficit disorder, and deficits in learning and memory [3–5,41].
301 There is growing evidence of links between circadian rhythms and both PFC function and many of
302 these neurobehavioral conditions [1,32,34,42,43]. Previous work from our group has demonstrated that
303 extracellular lactate (a functional output of neural metabolism) shows circadian rhythms in the medial
304 (m) PFC, and that ECD alters the morphology of medial mPFC neurons and affects PFC mediated

305 behaviors [13,44]. However, the studies presented here are the first to directly test whether cell
306 autonomous activity and synaptic inputs onto PFC neurons are rhythmic, define the mechanisms by
307 which this occurs, and investigate how circadian disruption impacts these functions.

308 Our finding that the resting state of plPFC neurons is more hyperpolarized during the dark period,
309 when the animals are awake and active, suggests that these neurons are less active and require a
310 higher degree of information input before eliciting a response and sending downstream signals to other
311 brain regions. On the surface, it seems counter-intuitive that plPFC pyramidal neurons would be more
312 inactive during the dark period, when these animals are active and engaging with their environment,
313 than the light (inactive) period. A functional hypothesis for this finding is that stronger gating during the
314 wake period serves as a necessary mechanism for selective informational throughput in response to
315 environmental stimuli. Information filtering is paramount to having a proper behavioral output, and too
316 low of a threshold may result in overactivation as the animal engages with its environment. For
317 example, pharmacological studies have demonstrated that activation of the plPFC with neurotensin
318 agonists or the sodium channel activator veratrine lead to anxiogenic behaviors, likely through
319 increased glutamate release [45–47]. Behaviorally, autism spectrum disorder mouse models, with
320 hyperactive ventral hippocampus to mPFC excitatory inputs, display impaired social memory that is
321 rescued by inhibition of this circuitry, supporting the notion that overactivation of these neurons may be
322 detrimental to appropriate outputs and their impact on behavior [48]. Notably, we discovered a large
323 increase in excitatory inputs onto plPFC pyramidal neurons during the active period. This is in line with
324 other studies demonstrating that in layer 2/3 cortical neurons, excitatory inputs are increased during
325 spontaneous wakefulness and sleep deprivation occurring during the light (inactive) period [49]. While it
326 seems contradictory that these neurons simultaneously receive more excitatory inputs and become
327 more hyperpolarized, it is aligned with the proposal that these neurons require stronger gating
328 mechanisms during the active period, as more information is being sent to these neurons. One potential
329 source of increased excitatory inputs during the active period are projections from the hippocampus, as
330 high-frequency stimulation in the CA1 region results in larger excitatory post-synaptic potentials during

331 the active period [50]. It is critical that these incoming stimuli are somewhat filtered so only the strongest
332 signals are relayed further downstream.

333 Neurophysiological sex differences in the PFC, and their respective behavioral outputs, are well
334 documented and partly attributed to differences in synaptic signaling [14,15]. While exploring the effects of
335 time-of-day on these fundamental properties of PFC cells, we fully embraced inclusion of both males
336 and females, given the significant work demonstrating that use of both sexes (particularly inclusion of
337 females) can reveal important new concepts and understanding about brain function [51]. While not
338 designed explicitly as a sex-differences study, our results demonstrate that female mice had less
339 excitatory inputs than males, yet these inputs resulted in much larger postsynaptic currents, likely due
340 to known sex differences in glutamate receptor expression and basal release [52]. There are also sex
341 differences in response to environmental and pharmacological stressors [53]. For example, when
342 compared to male rats, females can display a lower threshold for impaired working memory after PFC
343 injections of benzodiazepine inverse agonists that activate the stress system [54]. Further, there are clear
344 sex differences in mPFC dendritic growth, microglia activity, and astrocyte morphology in response to
345 stress [55]. It should be noted that there is a report that basal PFC glutamate release is higher in females,
346 which seems opposite to our findings, but is likely due to experimental differences, as these studies
347 differ in species, PFC layers, electrophysiological solutions, and time-of-day [16]. We speculate that if the
348 underlying mechanisms that mediate information throughput and plasticity are fundamentally different in
349 males and females, and the basal tone of excitatory inputs is relatively low in females, then time-of-day
350 changes in information filtering may not be as crucial to optimal plPFC function in female mice.

351 GABAergic interneurons are highly involved in PFC function and relay information between
352 multiple regions of the PFC [9,27,56]. In the hippocampus, GABAergic inputs onto CA1 pyramidal neurons
353 regulate action potential firing frequency in response to current injections, with a higher inhibitory tone
354 during the light cycle [57,58]. Significantly, we found that in the plPFC there was no effect of sex or time-of-
355 day on spontaneous inhibitory inputs. This suggests that presynaptic inhibitory and excitatory inputs are
356 not the primary regulator of resting state or information throughput in layer 2/3 plPFC pyramidal
357 neurons. Instead, this supports the notion that basal inhibitory tone remains relatively constant

358 throughout the 24h day and, in male mice, a postsynaptic cell endogenous mechanism is responsible
359 for maintaining optimal information filtering when these neurons are challenged by the large increase of
360 excitatory signals during the active period.

361 We also demonstrate that the strength (amplitude) of inhibitory inputs was stronger during the
362 dark (active) period, specifically in male mice. GABA receptors are made up of several subunits, and
363 interact with postsynaptic ion channels, and there are sex differences in both of these aspects of GABA
364 receptor structure/function [14,59]. After investigating GABAergic signaling localized at the synapse and
365 isolated from upstream activity, we confirmed that inhibitory postsynaptic currents are stronger early in
366 the dark period in male mice. Interestingly, female mice displayed a large increase in inhibitory inputs
367 and strength late in the light period, a finding that requires future studies to fully understand its
368 functional implications.

369 Our findings point toward a postsynaptic mechanism underlying daily changes in the physiology
370 of layer 2/3 plPFC pyramidal neurons. This prompted us to explore how time-of-day impacts intrinsic
371 postsynaptic properties such as ionic currents and overall conductance. At hyperpolarized voltage
372 steps below the reversal potential of K^+, time-of-day did have a modest impact on the conductance and
373 current density of plPFC pyramidal neurons in female mice between the transition from the dark to light
374 period. However, at depolarized voltages greater than the mean RMP and action potential threshold
375 there was no time-of-day effect. This further supports the hypothesis that while neurophysiological daily
376 rhythms do exist in plPFC pyramidal neurons of female mice, they have little impact on overall resting
377 state and information throughput in response to electrical activity and synaptic inputs. In contrast, there
378 was a large effect on the current density and conductance of pyramidal neurons in male mice.
379 Specifically, when these neurons were hyperpolarized below the equilibrium potential for K^+, we
380 discovered that current density increased throughout the light period, peaking between the late period
381 and early dark period. This effect translated into an overall increase in conductance, and given that
382 conductance was highest around the beginning of the active period, when these neurons are most
383 hyperpolarized, we posited that this was due to an increased number of open K^+ channels and the
384 outflow of K^+ cations (outward current). Consistent with this prediction, when we blocked K^+ channel

385 mediated outward currents (by replacing K^+ with Cs^+ in our internal recording solution), the time-of-day
386 effect on current density and conductance was completely abolished at voltages near or below the K^+
387 equilibrium potential. Although internal Cs^+ was not sufficient to block the time-of-day effect on current
388 density at depolarized voltage greater than the K^+ equilibrium potential, it greatly reduced overall
389 current density and conductance.

390 To understand the functional relevance of these postsynaptic changes in ion channel function
391 and resting state, it was necessary to determine how time-of-day impacts action potential dynamics as
392 action potential firing is a functional measure for information throughput. Notably, this measure changes
393 with time-of-day in the hippocampus, and in response to sleep deprivation in the PFC [57,60]. Action
394 potentials are dependent on voltage-gated ion channels, and changes in K^+ channel activity can alter
395 action potential firing threshold and kinetics. Consistent with our interpretation that, in male mice, there
396 is a stronger gating mechanism to filter incoming signals during the active period, we discovered that
397 the threshold for action potential firing was increased during the active period. These data suggest that
398 layer 2/3 plPFC pyramidal neurons are not only more hyperpolarized during the light period, but are
399 functionally more difficult to activate, requiring much larger depolarizations to elicit action potentials and
400 relay information downstream. Though somewhat speculative, this could affect a wide range of
401 behaviors, including emotionality, a notion supported by work demonstrating that pharmacological
402 activation of plPFC neurons induces anxiogenic activity in mice, and acute stress enhances
403 glutamatergic transmission in the PFC [10,45,47].

404 Circadian disruption has myriad consequences for whole-animal physiology. This ranges from
405 peripheral effects on metabolic and immune responses, such as increased body weight, altered sleep
406 [13,61,62]. Here we demonstrate that the consequences of circadian disruption extend to the functional
407 level, reducing information throughput of pyramidal neurons by increasing the threshold for action
408 potential firing, which is critical for communication with other brain regions, such as the hippocampus
409 and amygdala. GIRK channels play a demonstrated role in pyramidal neurons and interneurons
410 throughout the infralimbic and prelimbic cortices [15,27,28,63]. Dynamic changes in GIRK channels underlie
411 stress-induced deficits in cognitive flexibility, and decreased GIRK channel function can impair fear

412 learning, likely through altered communication between the PFC and hippocampus [28,64]. Our data
413 shows that ECD increases GIRK1/2 channel activity, and this tips the balance of inter-region
414 communication. Together, this work is in agreement with previous studies demonstrating the
415 relationship between GIRK channel function and cognitive flexibility, and demonstrates that altered
416 GIRK1 channel activity may serve as a substrate for the deficits in cognitive flexibility observed in ECD
417 mice [28,61,64].

418 It is now well accepted that the mPFC is heterogeneous at the anatomical and physiological
419 levels, with consequences for behavior [12]. Our work suggests that perhaps we need to incorporate
420 temporal heterogeneity, even when looking at the fundamental properties of cellular function in the
421 mPFC. Given the impact of time-of-day on neuronal function in the PFC, the mechanistic work
422 presented here also has significant implications for incorporating time-of-day into the application of
423 pharmacological and behavioral interventions for mental health disorders, and opens the door to similar
424 questions in brain regions outside the PFC. Combined, we believe this work uncovers how fundamental
425 aspects of circuit function can be impacted by time-of-day, and underlines the importance of
426 understanding how daily rhythms influence neural function. While we are not suggesting all studies
427 should be undertaken at many times of day, our findings underscore that if we are to build
428 comprehensive models of cell-circuit-behavioral outputs, we must appreciate the relevant variables that
429 impact the cells of interest, including biological time.
430

431 **Methods**

432 *Animals*

433 All animal procedures and experiments were approved by the University of Massachusetts
434 Amherst Institutional Care and Use Committee in accordance with the U.S. Public Health Service Policy
435 on Humane Care and Use of Laboratory Animals and the National Institutes of Health *Guide for the*
436 *Care and Use of Laboratory Animals*. Male and female wild-type mice (Charles River, Wilmington, MA,
437 USA) on a C57BL/6J background were used for these studies. All mice were group-housed in light-tight
438 housing boxes at 25°C, under a 12:12-hr light:dark (LD) cycle, with food and water available *ad libitum*.
439 For circadian desynchronization experiments mice were transferred to a 10:10h LD cycle and
440 acclimated for at least three weeks prior to experimentation. LD cycles in housing boxes were offset so
441 that experiments from each ZT bin occurred at the same external (real world) time each day. Mice ages
442 10-16 weeks were used for these studies. For electrophysiology studies mice were anesthetized in a
443 chamber with isoflurane before euthanasia by decapitation.

444

445 *Brain slice electrophysiology*

446 Two mice were simultaneously euthanized 1-hr prior to their ZT bin (i.e., mice were euthanized at
447 ZT23 for recording bin ZT0-4). After euthanasia, brains were immediately removed and the forebrain
448 was blocked while bathing in a 0-4°C oxygenated N-methyl-D-glucamine (NMDG) - 4-(2-hydroxyethyl)-
449 1-piperazineethanesulfonic acid (HEPES) cutting solution composed of (mM): 92 NMDG, 2.5 KCl, 1.25
450 NaH_2PO_4, 30 $NaHCO_3$, 3 sodium pyruvate, 2 thiourea, 20 HEPES, 10 $MgSO_4$, 0.5 $CaCl_2$, 25 glucose,
451 20 sucrose. Cutting solution was brought to pH 7.4 with ~17mL of 5M HCl [65]. The forebrains were
452 mounted adjacent to each other and sectioned simultaneously on a vibratome (VT1200S, Leica
453 Biosciences, Buffalo Grove, IL, USA) with a sapphire knife (Delaware Diamond Knives, Wilmington,
454 DE, USA) yielding roughly three slices containing the PFC from each (250-μm) per mouse. Slices were
455 transferred and allowed to recover for 30-45 min in room temperature recording artificial cerebrospinal
456 fluid (aCSF) solution composed of (mM): 124 NaCl, 3.7 KCl, 2.6 NaH_2PO_4, 26 $NaHCO_3$, 2 $CaCl_2$, 2
457 $MgSO_4$, 10 glucose. aCSF had a final pH of 7.3-7.4, osmolarity of 307-310 mOsmos, and was

458 continuously bubbled using 95% 0_2/5% $C0_2$. For recordings, brain slices were transferred to a perfusion
459 chamber containing aCSF maintained at 34-37°C with a flow rate of 1mL/min. Neurons were visualized
460 using an upright microscope (Zeiss Axoskop 2, Oberkochen, Germany). Recording electrodes were
461 back-filled with experiment-specific internal solutions as follows (mM): Current-clamp and spontaneous
462 (s) excitatory postsynaptic currents (EPSCs); 125 K-gluconate, 10 KCl, 10 NaCl, 5 HEPES, 10 EGTA, 1
463 $MgCl_2$, 3 NaATP and 0.25 NaGTP (liquid-junction potential (LJP) = ~14.5 mV; Predicted E_K = ~-95 mV).
464 Voltage-clamp spontaneous inhibitory postsynaptic currents (sIPSCs); 140 CsCl, 5 $MgCl_2$, 1 EGTA, 10
465 HEPES, 3 NaATP, and 0.25 NaGTP (LJP = ~4.2 mV). All internal solutions were brought to pH 7.3
466 using KOH (current-clamp and EPSC) or CsOH (IPSC) at 301-304 mOsm. EPSCs were recorded in the
467 presence of the GABA receptor antagonist bicuculline (30 μM). sIPSCs were recorded in the presence
468 the competitive α-amino-3-hydroxy-5-methyl-4-isoxazolepropionic acid (AMPA)/kainate receptor
469 antagonist 6-cyano-7-nitroquinoxaline-2,3-dione (CNQX; 10 μM), the selective N-Methyl-d-aspartate
470 (NMDA) receptor antagonist (2R)-amino-5-phosphonovaleric acid (APV; 50 μM), and the glycine
471 antagonist strychnine (2 μM). Miniature (m) IPSCs had the addition of the voltage-gated sodium
472 channel (VGSC) blocker tetrodotoxin (TTX; 1 μM). The selective GIRK1 channel agonist ML297 (10
473 μM) was prepared in 0.04% DMSO, which was also added to the aCSF for recordings measuring
474 GIRK1 channel function. Patch electrodes with a resistance of 3-5MΩ were guided to neurons with an
475 MPC-200-ROE controller and MP285 mechanical manipulator (Sutter Instruments, Novato, CA, USA).
476 Patch-clamp recordings were collected through a UPC-10 USB dual digital amplifier and Patchmaster
477 NEXT recording software (HEKA Elektronik GmbH, Reutlingen, Germany). All voltage-clamp recordings
478 were obtained at V_H= -70 mV. Current clamp voltage-step protocols were performed from the cell
479 endogenous resting membrane potential and used 500ms 10-pA steps from -100 pA to +190 pA.
480 Voltage clamp current-step protocols were performed from V_H= -70 mV, and used 10-mV steps from -
481 120 mV to +30 mV. All compounds were obtained from Tocris Cookson, Cayman Chemical, and Sigma
482 Aldrich.
483 Individual recording locations were plotted (with neurons outside of the target area excluded from
484 analysis) to qualitatively confirm an equal distribution of recording sites between Zeitgeber (ZT) bins 0-

485 4, 6-10, 12-16, and 18-22 (**Fig. 1 Extended Data 1A-D**). A small percentage (~20%) of all recorded
486 neurons had unique characteristics in resting membrane properties, spontaneous excitatory
487 postsynaptic currents (sEPSCs), and action potential dynamics that were independent of time-of-day
488 (hereafter Type II neurons; **Fig. 1 Extended Data 2A-I**). Most notably, compared to Type I (most
489 abundant) neurons, Type II neurons (less abundant) displayed a much higher action potential velocity
490 and hyperpolarizing decay current (**Fig. 1 Extended Data 2A,B**). They also had a more depolarized
491 resting membrane potential (RMP) and decreased action potential firing threshold (**Fig. 1 Extended**
492 **Data 2E,F**). Due to these clear qualitative and quantitative differences independent of ZT bin, and that
493 they represented a small proportion of recorded neurons, we excluded the far less abundant Type II
494 neurons from analysis in our following experiments.
495
496 *Statistical Analysis*
497 For sEPSCs, only neurons with holding currents not exceeding 100pA at V_H= -70mV for the 10-
498 min control period (input resistance > 70 MΩ) were studied further. Neurons were not considered for
499 further analysis if series resistance exceeded 50MΩ or drifted >10% during baseline. Rheobase was
500 calculated as the first current step to elicit an action potential and action potential dynamics (threshold,
501 decay tau, and half-width) were obtained from the first evoked action potential to avoid variance in ion
502 channel function due to repeated action potential firing. G*Power 3.0 software (Franz Faul, Uni Kiel,
503 Germany) was used to conduct our power analysis, for a *p* value of <0.05 with 90% power. Adequate
504 sample sizes were based upon expected effect sizes from similar experiments. Raw data files were
505 analyzed in the Patchmaster NEXT software or converted using ABF Utility (Synaptosoft) for analysis in
506 MiniAnalysis (Synaptosoft). N-values for analysis and presented in figures represent individual cells.
507 Where applicable, extreme outliers were identified using the ROUT method with a conservative Q =
508 0.5% and are included with an asterisk in the figure source data. To control for biological variability
509 between groups N = 4-8 mice per group was used, with exact N-values provided in figure source data.
510 Statistical comparison of effects between each time-period was made using a full model two-way

511 ANOVA (column, row, and interaction effects) unless otherwise noted. Statistics were calculated using

512 Prism 9 (Graphpad Software, San Diego, CA, USA).

Acknowledgements

We would like to acknowledge and thank Dr. James Peters at Washington State University for his invaluable input and discussions during the preparation of this manuscript.

Grants

This work was supported by a CAREER grant 1553067 by the National Science Foundation, and R01 DK119811 from the National Institutes of Health to INK.

Competing Interests

BLR and INK declare no competing financial interests.

524 **References**

525 1. Woodruff, E. R. *et al.* Coordination between Prefrontal Cortex Clock Gene Expression and
526 Corticosterone Contributes to Enhanced Conditioned Fear Extinction Recall. *eNeuro* **5**, (2018).
527 2. McCarthy, M. J. & Welsh, D. K. Cellular Circadian Clocks in Mood Disorders: *J. Biol. Rhythms*
528 (2012) doi:10.1177/0748730412456367.
529 3. Popoli, M., Yan, Z., McEwen, B. S. & Sanacora, G. The stressed synapse: the impact of stress and
530 glucocorticoids on glutamate transmission. *Nat. Rev. Neurosci.* **13**, 22–37 (2012).
531 4. Sotres-Bayon, F., Cain, C. K. & LeDoux, J. E. Brain Mechanisms of Fear Extinction: Historical
532 Perspectives on the Contribution of Prefrontal Cortex. *Biol. Psychiatry* **60**, 329–336 (2006).
533 5. Miller, E. K. & Cohen, J. D. An Integrative Theory of Prefrontal Cortex Function. *Annu. Rev.*
534 *Neurosci.* **24**, 167–202 (2001).
535 6. Kawaguchi, Y. & Kubota, Y. GABAergic cell subtypes and their synaptic connections in rat frontal
536 cortex. *Cereb. Cortex N. Y. N 1991* **7**, 476–486 (1997).
537 7. Radnikow, G. & Feldmeyer, D. Layer- and Cell Type-Specific Modulation of Excitatory Neuronal
538 Activity in the Neocortex. *Front. Neuroanat.* **12**, (2018).
539 8. Vertes, R. P. Interactions among the medial prefrontal cortex, hippocampus and midline thalamus
540 in emotional and cognitive processing in the rat. *Neuroscience* **142**, 1–20 (2006).
541 9. Saffari, R. *et al.* NPY+-, but not PV+- GABAergic neurons mediated long-range inhibition from infra-
542 to prelimbic cortex. *Transl. Psychiatry* **6**, e736 (2016).
543 10. Yuen, E. Y. *et al.* Acute stress enhances glutamatergic transmission in prefrontal cortex and
544 facilitates working memory. *Proc. Natl. Acad. Sci.* **106**, 14075–14079 (2009).
545 11. Zaitsev, A. V., Povysheva, N. V., Gonzalez-Burgos, G. & Lewis, D. A. Electrophysiological classes
546 of layer 2/3 pyramidal cells in monkey prefrontal cortex. *J. Neurophysiol.* **108**, 595–609 (2012).
547 12. Moorman, D. E., James, M. H., McGlinchey, E. M. & Aston-Jones, G. Differential roles of medial
548 prefrontal subregions in the regulation of drug seeking. *Brain Res.* **1628**, 130–146 (2015).

549 13. Karatsoreos, I. N., Bhagat, S., Bloss, E. B., Morrison, J. H. & McEwen, B. S. Disruption of circadian
550 clocks has ramifications for metabolism, brain, and behavior. *Proc. Natl. Acad. Sci.* **108**, 1657–1662
551 (2011).
552 14. Andrade, S. *et al.* Effect of progesterone on the expression of GABA(A) receptor subunits in the
553 prefrontal cortex of rats: implications of sex differences and brain hemisphere. *Cell Biochem. Funct.*
554 **30**, 696–700 (2012).
555 15. de Velasco, E. M. F. *et al.* Sex differences in GABABR-GIRK signaling in layer 5/6 pyramidal
556 neurons of the mouse prelimbic cortex. *Neuropharmacology* **95**, 353–360 (2015).
557 16. Pena-Bravo, J. I., Penrod, R., Reichel, C. M. & Lavin, A. Methamphetamine Self-Administration
558 Elicits Sex-Related Changes in Postsynaptic Glutamate Transmission in the Prefrontal Cortex.
559 *eNeuro* **6**, ENEURO.0401-18.2018 (2019).
560 17. Laroche, S., Jay, T. M. & Thierry, A.-M. Long-term potentiation in the prefrontal cortex following
561 stimulation of the hippocampal CA1/subicular region. *Neurosci. Lett.* **114**, 184–190 (1990).
562 18. Ferguson, B. R. & Gao, W.-J. PV Interneurons: Critical Regulators of E/I Balance for Prefrontal
563 Cortex-Dependent Behavior and Psychiatric Disorders. *Front. Neural Circuits* **12**, (2018).
564 19. Kalmbach, B. E. & Brager, D. H. Fragile X mental retardation protein modulates somatic D-type K+
565 channels and action potential threshold in the mouse prefrontal cortex. *J. Neurophysiol.* **124**, 1766–
566 1773 (2020).
567 20. Deng, W.-K., Wang, X., Zhou, H.-C. & Luo, F. L-type Ca2+ channels and charybdotoxin-sensitive
568 Ca2+-activated K+ channels are required for reduction of GABAergic activity induced by β2-
569 adrenoceptor in the prefrontal cortex. *Mol. Cell. Neurosci.* **101**, 103410 (2019).
570 21. Workman, E. R. *et al.* Rapid antidepressants stimulate the decoupling of GABA(B) receptors from
571 GIRK/Kir3 channels through increased protein stability of 14-3-3η. *Mol. Psychiatry* **20**, 298–310
572 (2015).
573 22. Bano-Otalora, B. *et al.* Daily electrical activity in the master circadian clock of a diurnal mammal.
574 *eLife* **10**, e68179 (2021).

575 23. Hablitz, L. M., Molzof, H. E., Paul, J. R., Johnson, R. L. & Gamble, K. L. Suprachiasmatic nucleus
576 function and circadian entrainment are modulated by G protein-coupled inwardly rectifying (GIRK)
577 channels. *J. Physiol.* **592**, 5079–5092 (2014).
578 24. van Aerde, K. I. & Feldmeyer, D. Morphological and Physiological Characterization of Pyramidal
579 Neuron Subtypes in Rat Medial Prefrontal Cortex. *Cereb. Cortex* **25**, 788–805 (2015).
580 25. Piette, C. *et al.* Intracellular Properties of Deep-Layer Pyramidal Neurons in Frontal Eye Field of
581 Macaque Monkeys. *Front. Synaptic Neurosci.* **13**, 725880 (2021).
582 26. Le Merre, P., Ährlund-Richter, S. & Carlén, M. The mouse prefrontal cortex: Unity in diversity.
583 *Neuron* **109**, 1925–1944 (2021).
584 27. Anderson, E. M., Demis, S., D'Acquisto, H., Engelhardt, A. & Hearing, M. The Role of Parvalbumin
585 Interneuron GIRK Signaling in the Regulation of Affect and Cognition in Male and Female Mice.
586 *Front. Behav. Neurosci.* **15**, 621751 (2021).
587 28. Anderson, E. M. *et al.* Suppression of pyramidal neuron G protein-gated inwardly rectifying
588 K+ channel signaling impairs prelimbic cortical function and underlies stress-induced deficits in
589 cognitive flexibility in male, but not female, mice. *Neuropsychopharmacol. Off. Publ. Am. Coll.*
590 *Neuropsychopharmacol.* **46**, 2158–2169 (2021).
591 29. Kaufmann, K. *et al.* ML297 (VU0456810), the First Potent and Selective Activator of the GIRK
592 Potassium Channel, Displays Antiepileptic Properties in Mice. *ACS Chem. Neurosci.* **4**, 1278–1286
593 (2013).
594 30. Lippiello, P., Hoxha, E., Tempia, F. & Miniaci, M. C. GIRK1-Mediated Inwardly Rectifying Potassium
595 Current Is a Candidate Mechanism Behind Purkinje Cell Excitability, Plasticity, and
596 Neuromodulation. *The Cerebellum* **19**, 751–761 (2020).
597 31. Hastings, M. H., Reddy, A. B. & Maywood, E. S. A clockwork web: circadian timing in brain and
598 periphery, in health and disease. *Nat. Rev. Neurosci.* **4**, 649–661 (2003).
599 32. Otsuka, T. *et al.* Adverse Effects of Circadian Disorganization on Mood and Molecular Rhythms in
600 the Prefrontal Cortex of Mice. *Neuroscience* **432**, 44–54 (2020).

601 33. Morris, C. J. *et al.* Endogenous circadian system and circadian misalignment impact glucose
602 tolerance via separate mechanisms in humans. *Proc Natl Acad Sci U A* **112**, E2225-34 (2015).
603 34. Bechtold, D. A., Gibbs, J. E. & Loudon, A. S. Circadian dysfunction in disease. *Trends Pharmacol*
604 *Sci* **31**, 191–8 (2010).
605 35. Karatsoreos, I. N. Effects of circadian disruption on mental and physical health. *Curr Neurol*
606 *Neurosci Rep* **12**, 218–25 (2012).
607 36. Chaudhury, D., Wang, L. M. & Colwell, C. S. Circadian regulation of hippocampal long-term
608 potentiation. *J Biol Rhythms* **20**, 225–36 (2005).
609 37. Loh, D. H. *et al.* Misaligned feeding impairs memories. *eLife* **4**, e09460 (2015).
610 38. Paul, J. R. *et al.* Circadian regulation of membrane physiology in neural oscillators throughout the
611 brain. *Eur. J. Neurosci.* **51**, 109–138 (2020).
612 39. Chrobok, L. *et al.* Daily changes in neuronal activities of the dorsal motor nucleus of the vagus
613 under standard and high-fat diet. *J. Physiol.* (2021) doi:10.1113/JP281596.
614 40. McMartin, L., Kiraly, M., Heller, H. C., Madison, D. V. & Ruby, N. F. Disruption of circadian timing
615 increases synaptic inhibition and reduces cholinergic responsiveness in the dentate gyrus.
616 *Hippocampus* **31**, 422–434 (2021).
617 41. Xu, P., Chen, A., Li, Y., Xing, X. & Lu, H. Medial prefrontal cortex in neurological diseases. *Physiol.*
618 *Genomics* **51**, 432–442 (2019).
619 42. Hou, Y. *et al.* Long-term variable photoperiod exposure impairs the mPFC and induces anxiety and
620 depression-like behavior in male wistar rats. *Exp. Neurol.* **347**, 113908 (2022).
621 43. Harkness, J. H. *et al.* Diurnal changes in perineuronal nets and parvalbumin neurons in the rat
622 medial prefrontal cortex. *Brain Struct. Funct.* **226**, 1135–1153 (2021).
623 44. Wallace, N. K., Pollard, F., Savenkova, M. & Karatsoreos, I. N. Effect of Aging on Daily Rhythms of
624 Lactate Metabolism in the Medial Prefrontal Cortex of Male Mice. *Neuroscience* **448**, 300–310
625 (2020).
626 45. Li, B., Chang, L.-L. & Xi, K. Neurotensin 1 receptor in the prelimbic cortex regulates anxiety-like
627 behavior in rats. *Prog. Neuropsychopharmacol. Biol. Psychiatry* **104**, 110011 (2021).

628 46. Petrie, K. A. *et al.* The Neurotensin Agonist PD149163 Increases Fos Expression in the Prefrontal
629 Cortex of the Rat. *Neuropsychopharmacology* **29**, 1878–1888 (2004).
630 47. Saitoh, A. *et al.* Activation of the prelimbic medial prefrontal cortex induces anxiety-like behaviors
631 via N-Methyl-D-aspartate receptor-mediated glutamatergic neurotransmission in mice. *J. Neurosci.*
632 *Res.* **92**, 1044–1053 (2014).
633 48. Phillips, M. L., Robinson, H. A. & Pozzo-Miller, L. Ventral hippocampal projections to the medial
634 prefrontal cortex regulate social memory. *eLife* **8**, e44182 (2019).
635 49. Liu, Z.-W., Faraguna, U., Cirelli, C., Tononi, G. & Gao, X.-B. Direct Evidence for Wake-Related
636 Increases and Sleep-Related Decreases in Synaptic Strength in Rodent Cortex. *J. Neurosci.* **30**,
637 8671–8675 (2010).
638 50. Besing, R. C. *et al.* GSK3 activity regulates rhythms in hippocampal clock gene expression and
639 synaptic plasticity. *Hippocampus* **27**, 890–898 (2017).
640 51. Shansky, R. M. & Murphy, A. Z. Considering sex as a biological variable will require a global shift in
641 science culture. *Nat. Neurosci.* **24**, 457–464 (2021).
642 52. Perry, C. J., Campbell, E. J., Drummond, K. D., Lum, J. S. & Kim, J. H. Sex differences in the
643 neurochemistry of frontal cortex: Impact of early life stress. *J. Neurochem.* **157**, 963–981 (2021).
644 53. Yuen, E. Y., Wei, J. & Yan, Z. Estrogen in prefrontal cortex blocks stress-induced cognitive
645 impairments in female rats. *J. Steroid Biochem. Mol. Biol.* **160**, 221–226 (2016).
646 54. Shansky, R. M. *et al.* Estrogen mediates sex differences in stress-induced prefrontal cortex
647 dysfunction. *Mol. Psychiatry* **9**, 531–538 (2004).
648 55. Bollinger, J. L., Salinas, I., Fender, E., Sengelaub, D. R. & Wellman, C. L. Gonadal hormones
649 differentially regulate sex-specific stress effects on glia in the medial prefrontal cortex. *J.*
650 *Neuroendocrinol.* **31**, e12762 (2019).
651 56. Hu, H., Gan, J. & Jonas, P. Fast-spiking, parvalbumin+ GABAergic interneurons: From cellular
652 design to microcircuit function. *Science* **345**, 1255263–1255263 (2014).

653 57. Fusilier, A. R. *et al.* Dysregulated clock gene expression and abnormal diurnal regulation of
654 hippocampal inhibitory transmission and spatial memory in amyloid precursor protein transgenic
655 mice. *Neurobiol. Dis.* **158**, 105454 (2021).
656 58. Albers, E. H., Walton, J. C., Gamble, K. L., McNeill, J. K. & Hummer, D. L. The dynamics of GABA
657 signaling: Revelations from the circadian pacemaker in the suprachiasmatic nucleus. *Front.*
658 *Neuroendocrinol.* **44**, 35–82 (2017).
659 59. Janeczek, P., Colson, N., Dodd, P. R. & Lewohl, J. M. Sex Differences in the Expression of the α5
660 Subunit of the GABAA Receptor in Alcoholics with and without Cirrhosis of the Liver. *Alcohol. Clin.*
661 *Exp. Res.* **44**, 423–434 (2020).
662 60. Yan, J. *et al.* Short-term sleep deprivation increases intrinsic excitability of prefrontal cortical
663 neurons. *Brain Res.* **1401**, 52–58 (2011).
664 61. Pearson, G. L., Savenkova, M., Barnwell, J. J. & Karatsoreos, I. N. Circadian desynchronization
665 alters metabolic and immune responses following lipopolysaccharide inoculation in male mice.
666 *Brain. Behav. Immun.* **88**, 220–229 (2020).
667 62. Phillips, D. J., Savenkova, M. I. & Karatsoreos, I. N. Environmental disruption of the circadian clock
668 leads to altered sleep and immune responses in mouse. *Brain. Behav. Immun.* **47**, 14–23 (2015).
669 63. Anderson, E. M., Demis, S., Wrucke, B., Engelhardt, A. & Hearing, M. C. Infralimbic cortex
670 pyramidal neuron GIRK signaling contributes to regulation of cognitive flexibility but not affect-
671 related behavior in male mice. *Physiol. Behav.* **242**, 113597 (2021).
672 64. Victoria, N. C. *et al.* G Protein-Gated K+ Channel Ablation in Forebrain Pyramidal Neurons
673 Selectively Impairs Fear Learning. *Biol. Psychiatry* **80**, 796–806 (2016).
674 65. Ting, J. T. *et al.* Preparation of Acute Brain Slices Using an Optimized N-Methyl-D-glucamine
675 Protective Recovery Method. *JoVE J. Vis. Exp.* e53825 (2018) doi:10.3791/53825.

676

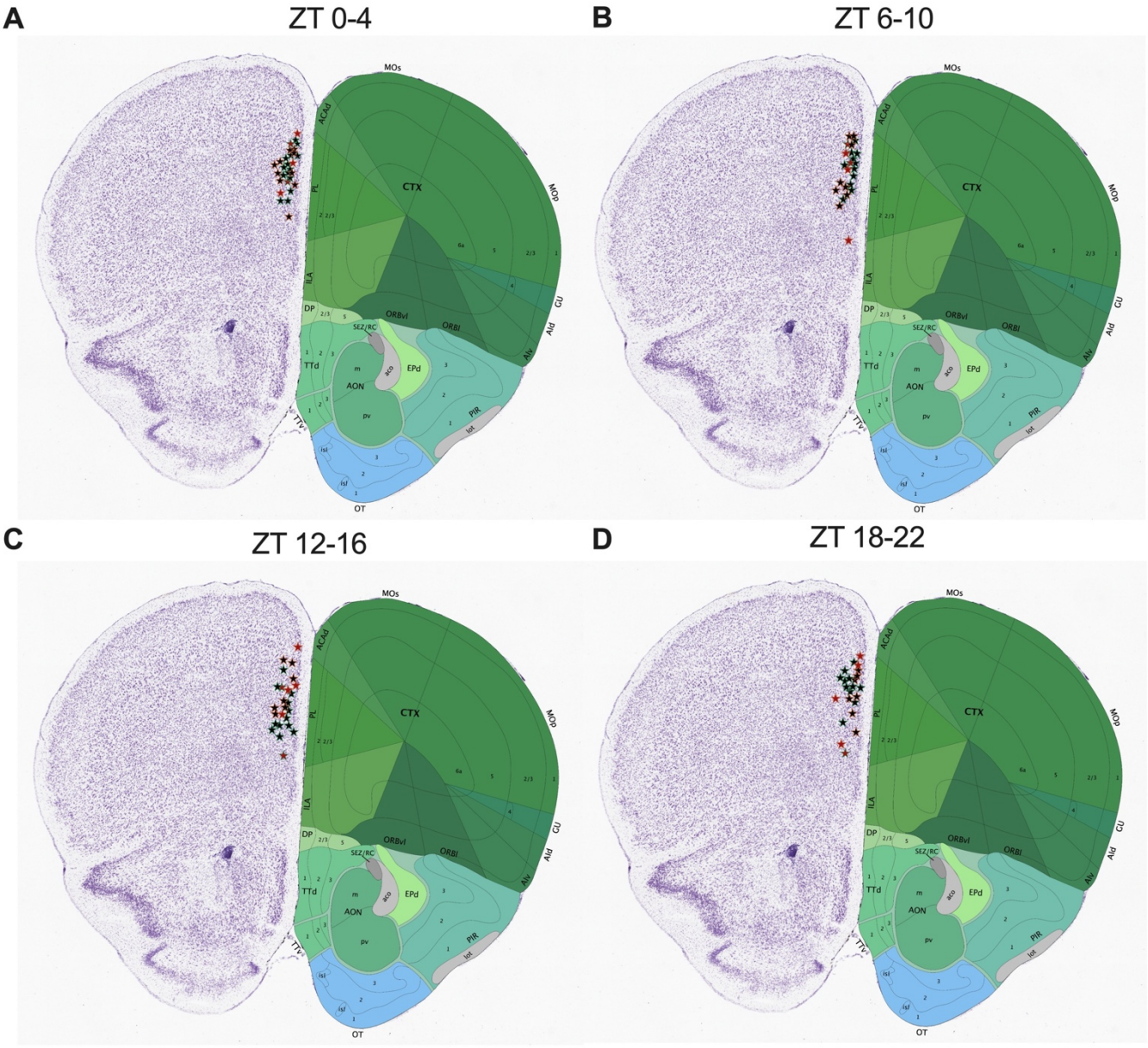

677

Figure 1 - Extended Data 1. *Recording map for layer 2/3 plPFC pyramidal neurons.* Coronal sections of forebrain showing individual recording sites from majority of neurons that were imaged at **(A)** ZT0-4, **(B)** 6-10, **(C)** 12-16 and **(D)** 18-22 for basal membrane property, sEPSC, and evoked action potential experiments in male (*bluish green outline*) and female (*vermillian outline*) mice. Stars filled with black represent 'Type I' neurons included for analysis and red stars represent Type II/III neurons excluded from analysis.

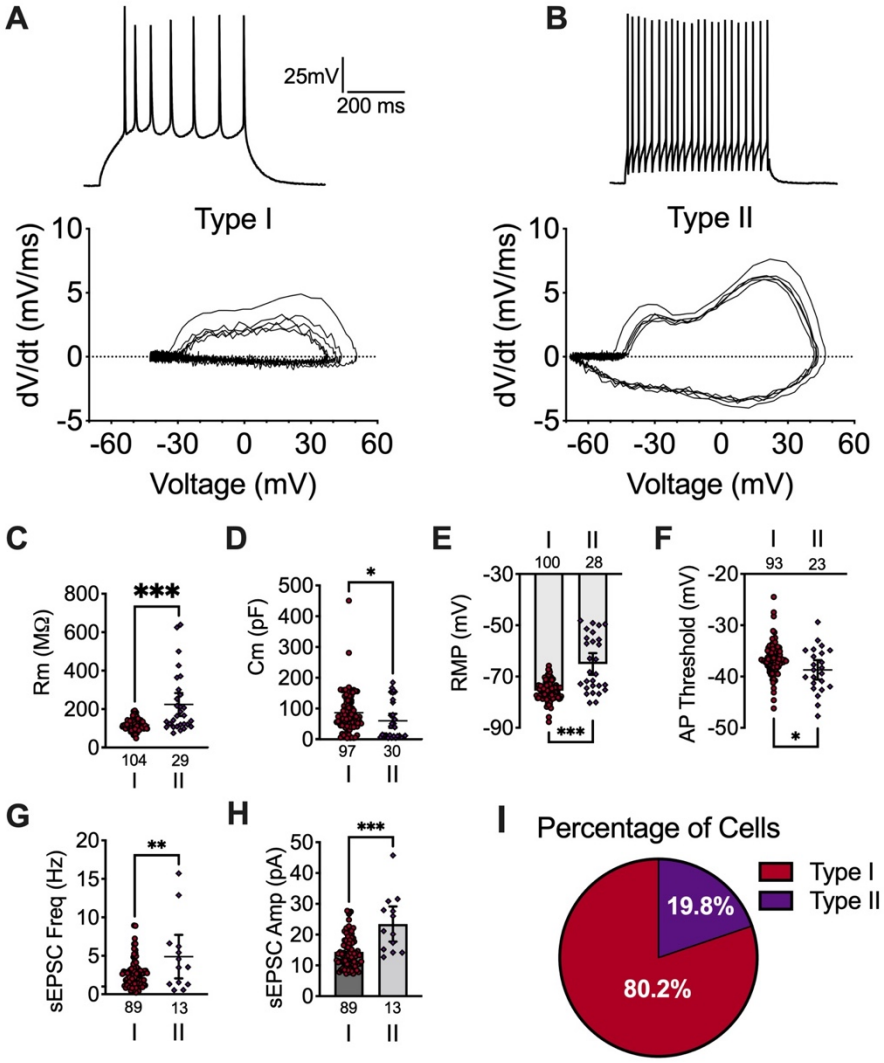

Figure 1 - Extended Data 2. *Categories and distinct physiological characteristics of plPFC neurons.* **(A)** Representative evoked action potential traces and phase plot diagram of first five action potentials (*bottom*) illustrating differences in velocity, trajectory, and amplitude in Type I and **(B)** Type II neurons. **(C)** Comparison of membrane resistance (Rm; t = 6.656, df = 131; *p* <0.001), **(D)** membrane capacitance (Cm; t = 2.003, df = 125; *p* = 0.05), **(E)** resting membrane potential (RMP t = 8.133, df = 126; *p* <0.001), **(F)** action potential (AP) threshold (t = 2.009, df = 114; *p* = 0.05), **(G)** sEPSC frequency (Freq; t = 3.267, df = 100; *p* = 0.001), and **(H)** sEPSC amplitude (Amp, t = 5.239, df = 100; *p* <0.001). **(I)** Percentage of recorded cells displaying Type I or Type II characteristics (combined among all ZT bins and sexes; calculated by *n* values from AP threshold). Error bars represent ± 95% CI. Unpaired student t-test, * *p< 0.05*, ** *p< 0.01*, ****p< 0.001*. Full analysis and data sets in **Figure 1 Extended Data 2 – Source**